Received: 29 April 2020 | Revised: 7 August 2020 | Accepted: 22 October 2020

IET Renewable Power Generation

DOI: 10.1049/rpg2.12114

The Institution of Engineering and Technology WILEY

REVIEW

Modern electric machines and drives for wind power generation: A review of opportunities and challenges

Hao Chen[1,#] | Yuefei Zuo[1,#] | K. T. Chau[2] | Wenxiang Zhao[3] | Christopher H. T. Lee[1]

[1] School of Electrical and Electronic Engineering, Nanyang Technological University, Singapore 639798

[2] Department of Electrical and Electronic Engineering, The University of Hong Kong, Hong Kong, China

[3] School of Electrical and Information Engineering, Jiangsu University, Zhenjiang 212013, China

Correspondence
Christopher H. T. Lee, School of Electrical and Electronic Engineering, Nanyang Technological University, Singapore 639798.
Email: chtlee@ntu.edu.sg

[#]Contributed equally to this work

Abstract

With ever-increasing concerns on energy crisis and environmental protection, there is a fast-growing interest in wind power generation systems. As electric machines and drives are core components in wind turbines, it is a pressing need for researchers and engineers to develop advanced electric machines and drives for wind power generation. This paper provides a thorough review of modern electric machines and drives for wind power generation, with emphasis on machine topologies, operation principles, performance characteristics, as well as control strategies. The key features of electric machines and drives including their merits and demerits, e.g. torque/power density, efficiency, and cost, are compared and summarised. Trade-offs involved in various presented methods and strategies are highlighted. The major challenges and difficulties, which electric machines and drives for wind power generation are facing, are discussed. Moreover, the developing trends and opportunities are revealed, while the latest development is also discussed.

1 | INTRODUCTION

Due to issues of energy security and environmental pollution associated with fossil fuels, focus of worldwide energy generation has been shifting to renewable energy sources, such as wind, solar, biofuels, and tidal streams. Among them, wind power generation is the fastest growing renewable energy source that has attracted more attention in both academia and industrial fields [1], [2]. The size of commercially available wind turbines has been exponentially increased over the past few decades, as depicted in Figure 1 [3].

Electric machines and drives are the key enabling technology for wind turbines. The required basic characteristics of an electric machine–drive system for wind power generation are shown as follows.

1. *High torque/power density:* As the generator is located on the top of tower, weight/volume of the generator system has more constraints than those used in other applications.
2. *High efficiency:* High efficiency is highly desirable in wind power generation systems so that the extracted energy from wind source can be converted as much as possible by reducing various electrical and mechanical losses.
3. *High reliability:* As wind turbines are usually installed at remote locations even offshore, access for maintenance/repair is challenging and very costly.
4. *Low cost:* Economical solution is one of the prime considerations especially when the price of high-energy rare-earth magnet has been dramatically soaring. Such magnet is one of the key enablers of modern permanent magnet (PM) machine technology used in wind power generation systems and many other applications.
5. *Flexible and readily controllability:* Due to intermittent and non-dispatchable nature of wind source, controlling a non-linear, strong-coupling, and multi-variable electric machine–drive system is challenging but imperative. It can, therefore, have the maximum possible energy and produce good-quality electrical power so as to meet the grid code requirements.

This paper provides a thorough review of modern electric machines and drives for wind power generation in terms of opportunities and challenges. In addition to more conventional machines, i.e. induction machines and conventional synchronous machines, new types of electric machines and their drives illustrating many attractive features for wind power generation are emphasised. Their merits and demerits in terms of

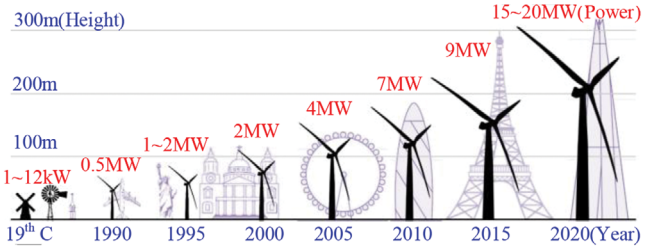

FIGURE 1 Evolution in height and power of wind turbines [3]

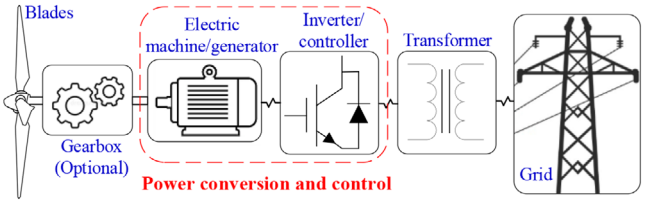

FIGURE 2 Basic configuration of a wind power generation system

torque/power density, efficiency, cost etc., are compared and summarised. Trade-offs involved in various presented methods and strategies are highlighted. Meanwhile, the major challenges and difficulties, which electric machines and drives for wind power generation are facing, are discussed. Moreover, the developing trends and opportunities are revealed, while the latest development is also discussed.

2 | WIND POWER GENERATION SYSTEMS

Wind power generation systems produce electricity by using wind power to drive an electric machine/generator. The basic configuration of a typical wind power generation system is depicted in Figure 2. Aerodynamically designed blades capture wind power movement and convert it into mechanical energy. Then, the electric machine/generator converts rotating mechanical energy into electric power, with an appropriate control strategy to extract the maximum possible energy and improve produced electric power quality. Afterwards, the produced electric power is transferred to grid through a transformer. As can be observed, the electric machine and drive play a key role in the wind power generation system for power conversion, which are the specific subject of this paper.

Based on their power delivering characteristics, electric machine–drive systems for wind power generation are generally classified into two types, i.e. fixed-speed electric machine–drive systems and variable-speed electric machine–drive systems.

2.1 | Fixed-speed electric machine–drive systems

Fixed-speed electric machine–drive systems have preliminarily led the way due to their simplicity, low initial cost, and reliable operation, as shown in Figure 3(a). Typically, a squirrel cage induction machine (SCIM) or a wound rotor induction machine (WRIM) is utilised as a generator, which operates in a narrow range (within ±1%) around the synchronous speed. The speed is determined by gear ratio and frequency of the supply grid, regardless of wind speed. Hence, the electric machine–drive system must be designed to achieve maximum efficiency at this particular generator speed. A gearbox is normally required to match wind speed and the generator. A soft starter is utilised to reduce inrush current when the generator is excited. In addition, since SCIMs or WRIMs always draw reactive power from the grid, a capacitor bank is usually employed for power factor compensation.

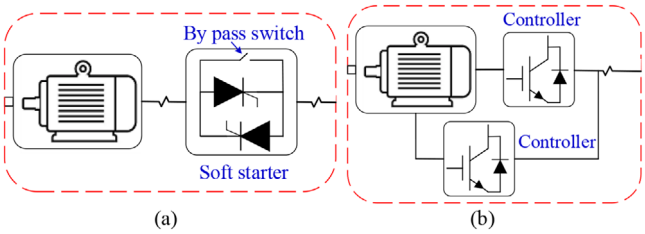

FIGURE 3 Electric machine–drive systems. (a) Fixed speed. (b) Variable speed

To improve wind source utilisation, pole-changeable SCIMs, which lead to two optional rotating speed, have been developed. 1-, 1.65-, and 2.3-MW SCIMs using the pole-changeable technology have become commercial solutions from manufacturers of Mitsubishi, Vestas, and Siemens, respectively [4].

Fixed-speed electric machine–drive systems were popular until two decades ago, while they are being replaced by variable-speed counterparts. This happens because of their inherent disadvantages of low wind energy conversion efficiency, inflexibilities in supporting grid voltage adjustment, inevitable power flicker, and mechanical stress issues due to wind gusts.

2.2 | Variable-speed electric machine–drive systems

In order to achieve maximum wind energy conversion efficiency over wide range of wind speed, the electric machine–drive system should be able to adjust its speed in accordance to wind speed so that the optimal tip-speed ratio can be obtained. Accordingly, variable-speed electric machine–drive systems, including semi-variable-speed systems and full-variable-speed systems, are drawing more attention. A power converter/controller is normally required to fulfil the high technical grid codes, while another controller is used for adjusting the speed of electric machine. A typical block diagram of a variable-speed electric machine–drive system is shown in Figure 3(b).

The main features of variable-speed systems include optimal wind energy conversion efficiency, quick response under transient/dynamic power system situations, and improved power quality. In addition, the need for gear box may be eliminated

TABLE 1 Comparison of fixed-speed and variable-speed systems

	Fixed-speed system	Variable-speed system
Speed range	±1% synchronous speed	0–100%
Power rating	2.3 MW (max)	>15MW
Gear box	Necessary	May be eliminated (direct-drive)
Control complexity	Simple	Complicated
Wind energy utilisation	Low	High
Produced power quality	Low since power flicker issues are inevitable.	High due to adjustment of power converter/ controller
Cost	Low	High
Suitable electric machines	Limited to SCIM or WRIM	Various induction machines (SCIM, WRIM, doubly fed IM) and synchronous machines (electrically or PM excited)
Examples	Vestas V82 [1]; Siemens SWT 2.3-101 [3].	Bard 5.0 [3]; Vestas V66/V-112 [6]; Enercon E126 [3]; Multibrid M5000 [6].

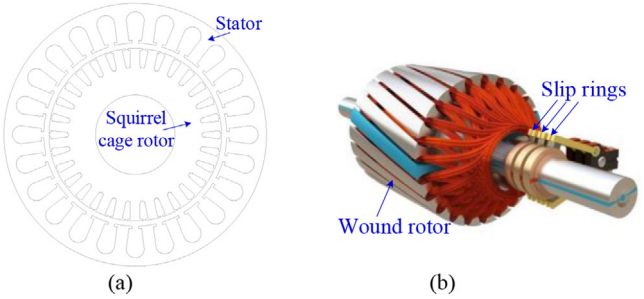

FIGURE 4 Induction machines. (a) SCIM. (b) Rotor of WRIM

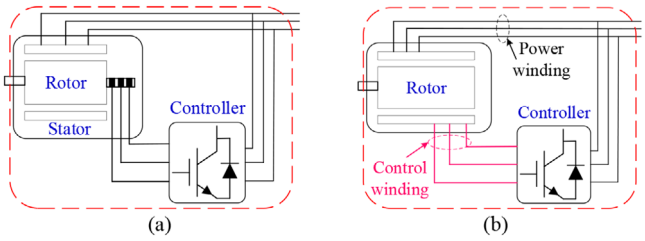

FIGURE 5 DFIMs. (a) Brushed [7]. (b) Brushless [11]

by using a high-pole number electric machine. Their disadvantages include increased losses from additional power electronic devices, as well as increased cost and control complexity [5].

Table 1 summarises the key differences between fixed-speed and variable-speed electric machine–drive systems. As can be seen, variable-speed systems have outperformed the fixed-speed counterparts in terms of flexibility and functionality, even though there are many fixed-speed systems still in operation that were installed long time ago.

3 | ELECTRIC MACHINE TOPOLOGIES FOR WIND POWER GENERATION

This section will cover the key publications addressing electric machine topologies for wind power generation, with emphasis on the novel PM machines, e.g. Vernier machines, flux-switching machines, flux-reversal machine, and magnetic-geared machines, in addition to conventional electrical machines.

3.1 | Conventional wind power generators

Conventional induction machines, i.e. SCIMs and WRIMs, have been preliminarily used in the electric machine–drive system for wind power generation. SCIMs are widely accepted candidates for wind turbines, due to their advantages of low cost, high reliability, and maintenance-free operation. SCIMs have a robust squirrel cage rotor containing aluminium or copper bars short-circuited at each end with shorting rings, as shown in Figure 4(a). Large current flows around the rotor bars, which creates magnetic field to interact with rotating magnetic field created by stator windings. However, the main disadvantages of SCIMs used in wind power generation include high starting current and poor starting torque. By contrast, in WRIMs, their rotor windings are connected through slip rings to external resistance, as shown in Figure 4(b). WRIMs can be started with low inrush current and high starting torque by adjusting external resistance. Moreover, WRIMs exhibit improved power factor compared to SCIMs. However, complication and regularly required maintenance associated with brushes and ship rings are the main disadvantages of WRIMs. Conventional induction machines, including SCIMs and WRIMs, are normally used in fixed-speed electric machine–drive systems. Since these machines consume reactive power from the grid to continue their generation operation, complex power factor correction control schemes are needed.

Developing based on WRIMs, doubly fed induction machines (DFIMs) become more popular in wind power generation. DFIMs consist of a WRIM with a wound rotor and a slip ring assembly with brushes connected to a controller, instead of external resistance, as shown in Figure 5(a) [7]. The stator windings of DFIMs are connected to the grid, while the rotor windings are connected to the controller, which controls both rotor and grid currents. Input current in the rotor is adjusted in frequency and phase angle to compensate for speed variations of the turbine. Moreover, active and reactive power fed to the grid can also be optimised by this adjustment. Hence, DFIMs are suitable for variable-speed electric machine–drive systems. In order to avoid the issues associated with brushes and slip rings, brushless DFIMs have attracted extensive attention since they are first proposed in [8]. Various brushless DFIM versions have been developed from conventional cascaded machines to self-cascaded machines and to modern DFIMs [9], [10].

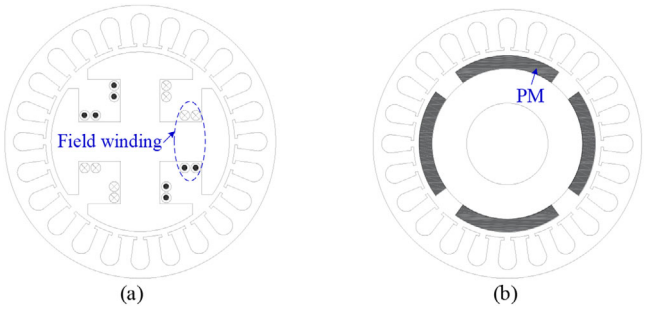

FIGURE 6 Synchronous machines. (a) EESM. (b) PMSM

Differing from conventional DFIMs, contemporary brushless DFIMs consist of two sets of stator windings, i.e. power windings and control windings, as shown in Figure 5(b) [11]. Power windings are connected to the grid, while control windings are supplied through a converter/controller in a "back-to-back" configuration for bidirectional power flow. The rotor, which takes a special "nested" cage structure or a reluctance form, produces shaft position-dependent magnetic coupling between the two sets of stator windings for torque production. With absence of rotor windings, brushless DFIMs have the advantages of enhanced reliability and maintenance-free operation, as well as flexible control of active and reactive power, showing their promising prospects in variable-speed electric machine–drive systems. Although brushless DFIMs have gone through several decades of evolution, research works on brushless DFIMs still lie on the initial stage. It is because practical implementation of brushless DFIMs is very challenging due to complexity of power control.

Compared to asynchronous induction machines mentioned above, synchronous machines, which includes electrically excited synchronous machines (EESMs) and permanent magnet synchronous machines (PMSMs), have potential to be used in direct-drive wind turbines. With elimination of gearbox, direct-drive wind power generation systems exhibit reduced manufacturing cost and gear-associated noise. Moreover, required regular maintenance for gearbox is eliminated. The EESM was first introduced with a power rating of 0.5 MW in direct-drive variable-speed wind turbines by Enercon of Germany in 1992 [12]. As depicted in Figure 6(a), the stator of EESMs is the same as that of induction machines, while the rotor may be salient or cylindrical wound by field windings that are excited by a direct current (DC) source through brushes and slip rings or a rotating rectifier. By contrast, air-gap magnetic field excitation is provided by PMs in PMSMs, as shown in Figure 6(b). PMSMs are gaining more interests due to their inherently high power density, high efficiency, and high reliability.

Table 2 provides a high-level summary of the key points among these conventional electric machines. Surveys show that about 48.6% of wind turbines used in industry are DFIMs, 48.1% are SCIM based, while 3.2% are PMSM based and other types account for about 0.1% [1]. As can be seen, although more than 90% of existing wind turbines are equipped with induction machines, PMSMs are the most promising candidate in wind power generation systems due to their aforementioned distinct advantages. With the improvement in PM performance and development of advanced power electronics, many manufacturers, e.g. General Electric, Vestas, Multibird, Win-Wind, and Siemens, are attempting to switch from induction machines to PMSMs [3], [6]. Based on conventional surface-mounted PMSMs, as shown in Figure 6(b), the number of new entrants/variants of PMSMs is growing rapidly, which shall be detailed in the later part of this section.

3.2 | Vernier PM machines

Vernier PM machines have gained increasing attention due to their high torque density and simple mechanical structure. A typical Vernier PM machine is depicted in Figure 7(a). As can be seen, the Vernier PM machine has a similar structure with a conventional surface-mounted PMSM [refer to Figure 6(b)] in terms of topology. However, in conventional PMSMs, the number of stator poles is the same as the number of rotor poles, while the number of stator poles of Vernier PM machines is different from the number of rotor poles. Generally, Vernier PM machines are equipped with a relatively small number of stator poles and much larger number of rotor poles to emphasise its Vernier effect. A small movement of PM rotor produces a large movement of flux linkage in stator armature windings. As the rotor steps down from speed of rotating field, torque steps up. Hence, Vernier PM machines are attractive in low-speed high-torque applications, e.g. wind power generation [21].

In [22], Yu et al. designed a double-stator toroidal-winding Vernier PM machine for wind power generation, as shown in Figure 7(b). In this machine, toroidal windings twist on both inner and outer stators, with cup rotor locating in the middle. It was shown that the optimal machine topology contributes to this machine with high power density and low torque ripple. Moreover, the rated voltage can be maintained with high modulation continuity under speed variations through appropriately selecting operating modes by integrating the toroidal winding configuration and terminal connection diversities.

Outer-rotor machines are generally superior to conventional inner-rotor counterparts due to better heat dissipation and easier installation especially in direct-drive operations. In [23], Zhang et al. presented an outer-rotor Vernier PM machine, as shown in Figure 7(c). In [24], Li et al. presented an outer-rotor Vernier PM machine with a toothed-pole stator for wind power generation, as shown in Figure 7(d), whose stator tooth is split into three small teeth at the end. It was shown that these outer-rotor Vernier PM machines can offer low-speed operation to directly capture wind power and enable high-speed rotating field design to maximise power density. Moreover, the toothed-pole stator in Figure 7(d) benefits this machine to achieve higher power density and output voltage, as well as reduce raw material volume and hence overall cost. All these features show promising prospects for wind power generation. In [25] and [26], Kim et al. presented an outer-rotor Vernier PM machine with concentrated windings for wind power generation. It was found that the power factor of this machine sharply deteriorates as the machine volume decreases, while the

TABLE 2 Comparison of conventional electric machines in wind power generation

	SCIM	WRIM	DFIM	Brushless DFIM	EESM	PMSM
Speed range	**Fixed/semi-variable speed**	**Fixed/semi-variable speed**	**Variable speed**	**Variable speed**	**Variable speed**	**Variable speed**
Gearbox requirement	**Yes**	**Yes**	**Yes**	**Yes**	**Optional**	**Optional**
Torque density	Low since magnetic field excitation only comes from the stator current [13].	Medium since the externally excited rotor current can provide additional field excitation [1].	Medium since the externally excited rotor current can provide additional field excitation [7].	High due to the presence of both asynchronous and synchronous torque components [9].	Low since the electrically excited rotor are bulky [14].	Highest due to the high-energy PM [12].
Maintenance requirement	Low due to the simple and robust structure [13].	High since the brushes and slip rings need regular maintenance.	High since the brushes and slip rings need regular maintenance [11].	Low due to the absence of brushes and slip rings [11].	High since the brushes and slip rings need regular maintenance [14].	Relatively low due to the relatively simple and robust structure [3].
Power quality	Low since power flicker is inevitable and it consumes reactive power from the grid [6].	Low although it also consumes reactive power from the grid, it shows low inrush current and improved power factor [1].	High due to their flexibility and ability to control active and reactive power [10].	High due to their flexibility and ability to control active and reactive power [10].	High due to the more sinusoidal output voltage waveform, low voltage regulation, and improved power factor [1].	High due to the more sinusoidal output voltage waveform, low voltage regulation, and improved power factor [1].
Efficiency	Low due to the high joule losses resulted from both the stator and rotor currents, and high core losses [3].	Low due to the high joule losses, core losses, and additional heat losses from the external resistance [3].	High since there is no additional heat losses from the external resistance [7].	High since there is no heat losses from the brushes and slip rings, as well as the external resistance [9].	Medium due to relatively low core losses, but there is heat losses from brushes and slip rings [14].	Highest due to relatively low core losses and no heat losses from brushes and slip rings [12].
Reliability	Highest due to the simple and robust structure [13].	Low since brushes and slip rings are required.	Low since brushes and slip rings are required [11].	Medium due to the absence of brushes and slip rings, but additional control windings are required [11].	Low since brushes and slip rings are required for rotor current excitation [12].	High due to the absence of the brushes, slip rings, and additional control windings [12].
Cost	Lowest due to the cheap materials [1].	Low due to the cheap materials but additional brushes and slip rings [14].	Medium due to the additional brushes and clip rings and additional power electronic devices [7].	High due to the additional control windings and the additional power electronic device [1].	Medium due to the additional devices for rotor current excitation [15].	Highest due to expensive PM [12].
Examples	Vestas V82-1.65 MW [3]. Siemens SWT-101-2.3 MW [3].	Vestas V80-1.8 MW [1]. Suzlon S88-2.1 MW [3].	Suzlon S70 (1.5 MW) [16]. Vestas V80-2.0 MW [14]. Gamesa SG 145-5.0 MW [17].	ATW-26-275 kW [1].	Enercon E-33 (300 kW) [13]. Enercon E-82-E3 (3MW) [18]. Enercon E-126-7.5MW [19].	Aeolia D2CF-200 kW [20]. Vestas V90 Grid (2.0 MW) [20]. Siemens SWT-154-7.0 MW [14].

machine volume depends on the number of stator toothed-poles.

Compared to the conventional three-phase counterparts, multi-phase machines have the advantages of high power density, high fault-tolerant capability, and additional degrees of freedom in the associated control system [27]. In [28], Song and Liu presented a six-phase Vernier PM machine as a direct-drive generator, as shown in Figure 7(e). This machine has double windings, i.e. armature windings and harmonic windings. The six-phase armature windings are concentrated, while the harmonic windings are wound in the stator toothed-poles in order to suppress the harmonic contents of inducted voltage. It was found that with the harmonic windings, total harmonic distortion (THD) of this machine is reduced from 4.52% to 1.96% under no-load condition.

In [29], Wang et al. presented a hybrid excited Vernier PM machine for wind power generation, as shown in Figure 7(f). In this machine, two sets of windings are employed in stator slots, where one is three-phase alternating current (AC) windings and the other one is six-phase DC windings. It was shown

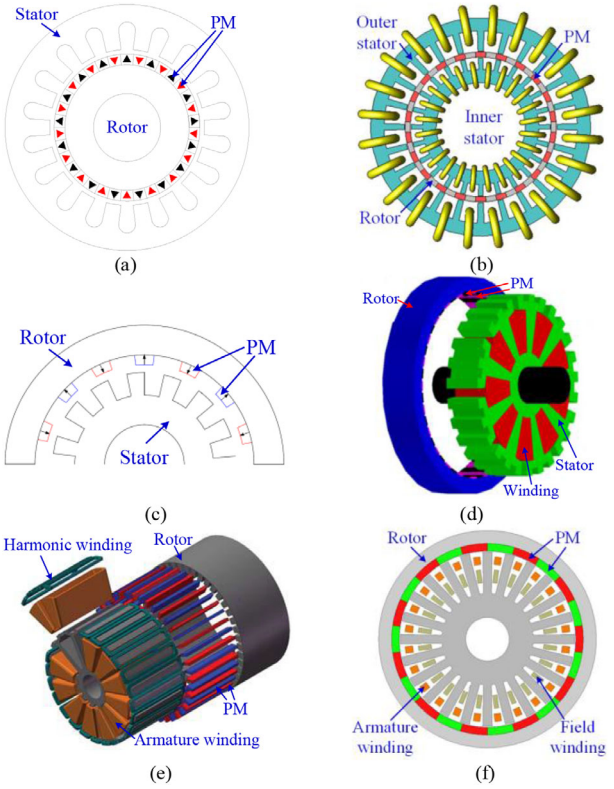

FIGURE 7 Vernier PM machines. (a) Classical Vernier PM machine. (b) Double-stator toroidal-winding Vernier PM machine [22]. (c) Outer-rotor Vernier PM machine [23]. (d) Outer-rotor Vernier PM machine with toothed-pole stator [24]. (e) Six-phase Vernier PM machine with harmonic windings [28]. (f) Hybrid excited Vernier PM machine [29]

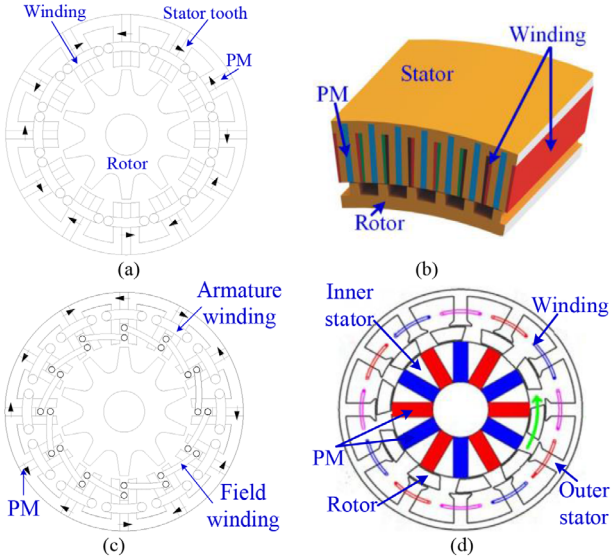

FIGURE 8 FSPM machines. (a) Classical FSPM machine [30]. (b) 120/100-p FSPM machine [31]. (c) Hybrid excited FSPM machine [37]. (d) Partitioned-stator FSPM machine [39]

that besides the original harmonic components used to induce sinusoidal back-electromotive force (EMF) in the AC windings, another low-order harmonic component can also be generated. Hence, this machine generates AC and DC power simultaneously, which is very suitable to be used as wind generator for the hybrid AC/DC microgrid in distributed generation systems.

3.3 | Flux-switching PM machines

Differing from the conventional PMSMs where their PMs are located on their rotor, flux-switching PM (FSPM) machines have PMs on their stator. A classical FSPM machine is shown in Figure 8(a) [30]. As can be seen, the rotor of FSPM machines is mechanically robust due to simple structure. The stator contains laminated "U"-shape stator tooth segments, circumferentially magnetised PMs, and concentrated windings. FSPM machines are gaining interest over the last few decades due to their high torque density, favourable thermal management of PMs, and essentially sinusoidal back-EMF.

In order to eliminate gearboxes, a large number of poles are required in direct-drive wind power generation systems. In [31], Ojeda et al. presented a 120/100-p (stator/rotor-pole) FSPM generator, as shown in Figure 8(b). It was shown that a direct-drive FSPM generator is very competitive and possibly the best solution for small-scale wind turbines, which typically used in rural systems, small farms, and villages.

In [32], Li et al. designed a nine-phase FSPM machine for wind power generation. Three topologies with different stator/rotor-pole combinations, i.e. 18/16-p, 18/17-p, and 36/34-p, are investigated. It was shown that compared to the 18/16-p counterpart, cogging torque of the 18/17-p and 36/34-p machines can be almost negligible, while the 18/17 machine has the highest PM utilisation. In [33], Shao et al. conducted a comparative study for a nine-phase FSPM machine and a 12-phase FSPM machine for wind power generation. It was shown that the 12-phase 24/22-p FSPM machine exhibits higher air-gap flux density, higher torque/power density, and lower voltage regulation factor. Then, a mathematical model for this 12-phase 24/22-p FSPM machine was developed in [34]. It was found that compared to conventional three-phase counterparts, mutual inductances of the 12-phase FSPM machine are much smaller and most of them are negligible. This brings benefit of improved magnetic isolation between phases. Building upon this model, effect of phase shift between winding sets and rotor-pole number on electromagnetic performance of the 12-phase FSPM machine was investigated in [35] and [36], respectively. It was found that the optimal phase shift for the lowest torque ripple and output rectified voltage oscillation depends on winding types, while symmetrical phase shift is not always appropriate for all occasions. More specifically, for even-multiple odd-phase windings, asymmetric phase shift is superior to the symmetrical one in terms of reduced torque ripples. In addition, by comparing with the 20-, 22-, 26-, and 28-rotor-pole FSPM machines, the 24/26-p FSPM machine exhibits the highest average torque and efficiency, while the 24/22-p machine has the smallest cogging torque and torque ripple, as well as relatively good voltage regulation and efficiency. All these features are essential for wind generators.

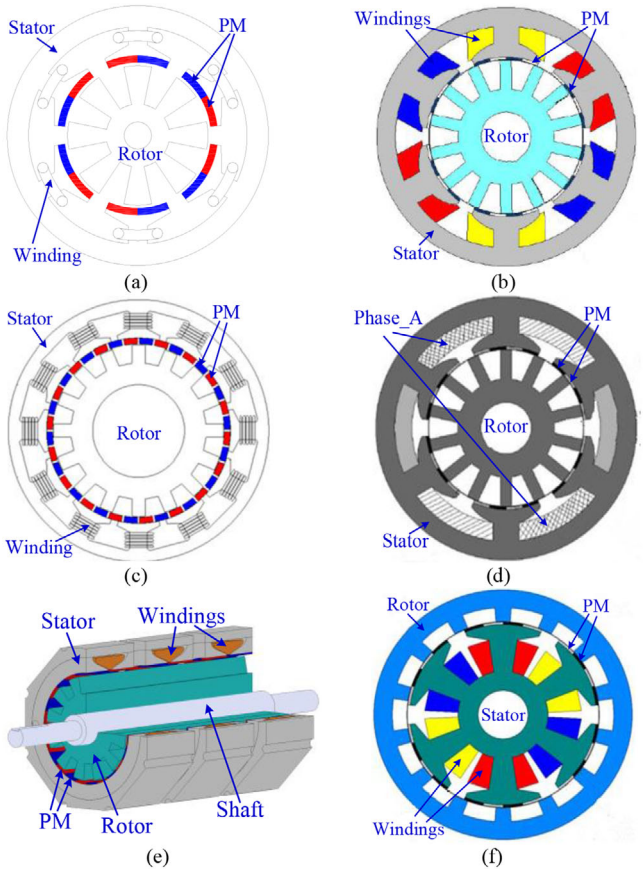

FIGURE 9 FRPM machines. (a) Classical FRPM machine [41]. (b) 6/14-p FRPM machine [43]. (c) FRPM machine with evenly distributed PMs [45]. (d) FRPM machine with distributed windings [46]. (e) Soft magnetic composite FRPM machine [48]. (f). Outer-rotor FRPM machine [49]

In [37] and [38], Wang et al. presented a hybrid excited FSPM machine for wind power generation, as shown in Figure 8(c). This machine combines the advantages of both PM machines and electrically excited machines, where it shows improved flux-enhancing capability and flux-weakening capability.

Differing from the conventional FSPM machine topology, as shown in Figure 8(a), a partitioned-stator FSPM machine is presented for wind power generation, as depicted in Figure 8(d) [39], [40]. The partitioned-stator FSPM machine purposely separates its windings and PMs in different stator in a sense both components are not competing space in the same stator. Consequently, as compared to the conventional topology, the partitioned-stator FSPM machine exhibits higher torque density, efficiency, and PM utilisation ratio.

3.4 | Flux-reversal PM machines

Flux-reversal PM (FRPM) machines have been gaining interest over the past few years due to the advantages of simple rotor configuration, fast transient response, and high power density. A classical FRPM machine is shown in Figure 9(a) [41]. As can be seen, the rotor of the FRPM machine is also mechanically robust as FSPM machines. A pair of PMs with alternate polarities is mounted on the inner surface of each stator tooth. Besides, the tooth windings are usually wound around the stator teeth, resulting in short end windings. When the rotor rotates, for each stator tooth, the areas of the two PM segments directly facing the rotor teeth vary against the rotor position, resulting in bipolar flux and back-EMF waveforms in the tooth windings.

In [42] and [43], More et al. presented a 6/14-p FRPM machine for direct-drive-rooftop wind power generation, as shown in Figure 9(b). It was found that differing from conventional PMSMs, which have same number of stator and rotor poles, FRPM machines have different number of stator and rotor poles, while the 6/14-p FRPM machine can be viewed as a two-pole PMSM with an inbuilt fictitious electrical gear (gear ratio is 14). Moreover, this FRPM machine shows higher power density than a fractional-slot concentrated-winding PMSM counterpart.

In [44], Li et al. also presented a 6/14-p FRPM machine with a power rating of 1.1 kW at 214 r/min for wind power generation, which contains the advantage of the switched reluctance machine and conventional PMSM into one machine. A simple method for calculation of end-effects is also presented to modify the 2-D method predicted results so that it gets closer to the results with the actual prototype.

In [45], Li et al. developed an FRPM machine with evenly distributed PMs for wind power generation, as shown in Figure 9(c). In this machine, the PMs are evenly distributed along the inner surface of the stator. It was shown that compared to the conventional FRPM counterpart, this machine exhibits 33% higher average torque, 78% lower cogging torque, and 72% lower torque ripple.

In [46] and [47], More et al. designed a full-pitched distributed winding FRPM machine for wind power generation, as shown in Figure 9(d). Compared to the conventional FRPM counterpart with concentrated windings, the no-load induced voltage of this machine is doubled, and its power density and efficiency are also improved. However, the voltage regulation of this machine is relatively poor, due to the high armature reaction. Hence, additional capacitors are needed to improve the voltage regulation.

In [48], Dmitrievskii et al. presented a soft magnetic composite FRPM machine for wind power generation, as shown in Figure 9(e). As can be seen, the stator core is in the form of a solid of revolution with three slots containing the three-phase toroidal windings. Compared to the conventional PMSM counterpart, this machine exhibits high power density and low cost.

Furthermore, an outer-rotor FRPM machine is designed for wind power generation in [49], as shown in Figure 9(f). It was found that this machine has 1.25 times higher torque density than the inner-rotor counterpart for the same machine outer dimensions and number of turns.

3.5 | Magnetic-geared PM machines

Magnetic-geared PM machines come from the concept of magnetic gear, which is shown in Figure 10(a). Magnetic gear is able to transmit torque between an input and an output shaft

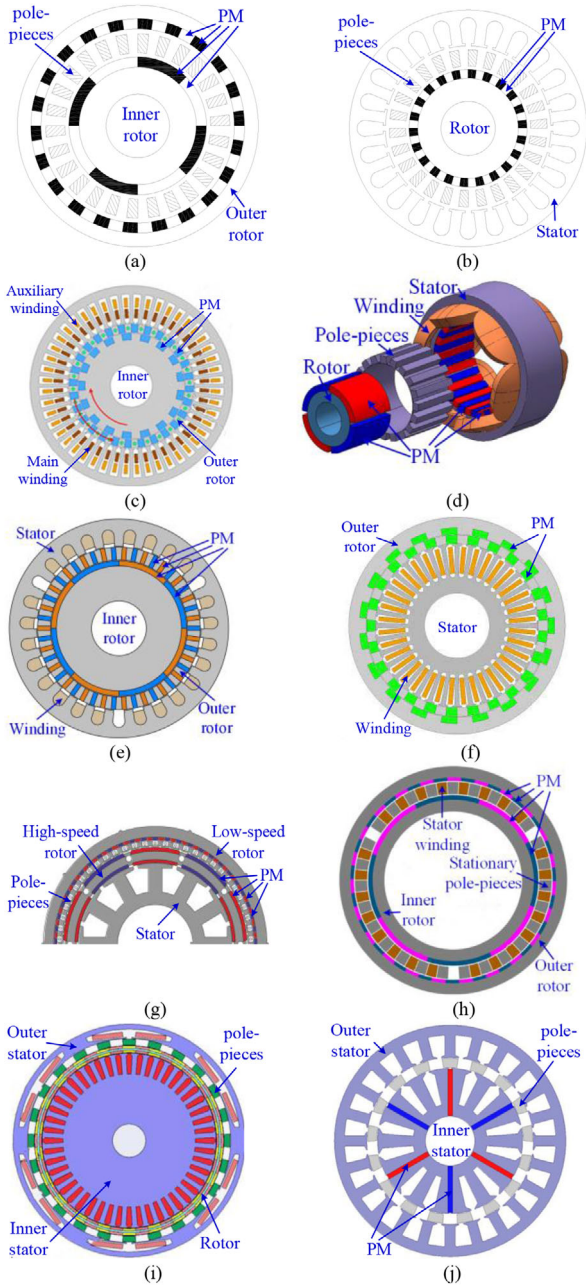

FIGURE 10 Magnetic-geared PM machines. (a) Magnetic gear [50]. (b) Classical magnetic-geared PM machine. (c) Doubly fed magnetic-geared PM machine [53]. (d) Magnetic-geared PM machine with PM fixed on stator surface [54]. (e) Stator-modulating magnetic-geared PM machine [55]. (f) Outer-rotor counterpart of the machine in (e) [56]. (g) Outer-rotor magnetic-geared PM machine [57]. (h) Magnetic-geared PM machine with a sandwiched armature stator [59]. (i) Double-stator magnetic-geared PM machine [60]. (j) Double-stator pole-changing magnetic-geared PM machine [61]

without mechanical contact, whose principle of operation is based on modulation of magnetic fields produced by two PM rotors via ferromagnetic pole pieces [50]. As shown in Figure 10(b), the magnetic-geared PM machine artfully incorporates a magnetic gear into a surface-mounted PM machine. In this machine, armature windings in stator and PMs on rotor are designed to be with different pole numbers so as different speeds. The rotating ferromagnetic pole pieces play as a flux modulator matching the two magnetic fields from stator and rotor to have same pole number and same speed. Thus, there is a steady torque production as a reduction gear does, leading to achieve low-speed high-torque direct-drive function that is favourable in wind power generation. Several magnetic-geared PM machines have been presented for wind power generation [51], [52]. It was shown that magnetic-geared PM machines outperform conventional PMSMs in terms of torque density.

In [53], Luo and Niu designed a doubly fed magnetic-geared PM machine for wind power generation, as shown in Figure 10(c). The outer rotor serves as the main rotor that is connected with blades, while the inner rotor is connected with auxiliary blades to compensate for wind energy absorption. These two rotors rotate in opposite directions. Induced frequency in the main winding of the generator is almost doubled due to the relative angular speeds. This phenomenon is based on the flux-modulation theory, which is desired in wind power generation systems. Torque of dual rotors can be controlled with the main and auxiliary windings. Hence, maximum wind energy conversion efficiency can be achieved with an appropriate control strategy.

In [54], Tlali et al. presented a magnetic-geared PM machine with PM fixed on stator surface for wind power generation, as shown in Figure 10(d). It was found that its torque density can reach as high as 70 N·m/L, which is significantly higher than that of conventional electric machines.

Zhang et al. [55] and Wang et al. [56] presented a stator-modulating magnetic-geared PM machine and an outer-rotor counterpart, as shown in Figure 10(e) and (f), respectively. Differing from the conventional magnetic-geared PM machine, as shown in Figure 10(b), the middle rotors of these machines are equipped with PMs, while the stator with modulating teeth plays the same functional role as ferromagnetic pole pieces in conventional magnetic-geared PM machines. The ferromagnetic pole pieces in the middle rotor between the PMs provide flux paths not only for the outer PMs, but also for the inner PMs. It was found that this machine is able to allow all PMs on the two rotors to perform energy conversion with armature windings. Hence, good torque capability and power factor are achieved, which are desired in wind power generation.

In [57], Kjaer et al. developed an outer-rotor magnetic-geared PM machine for direct-drive wind power generation, as shown in Figure 10(g). As can be seen, it is a straight-forwardly integrated magnetic-geared PM machine system that comprises a magnetic gear (outer part) and a surface-mounted PMSM (inner part). The outer magnetic gear part with 106 low-speed poles is directly driven by blades, while the inner PMSM part with 10 high-speed poles, which is modulated by 58 pole pieces, plays as a generator. In [58], Jian et al. also presented an outer-rotor magnetic-geared PM machine for wind power generation. The advantages of smaller size and lighter weight for these outer-rotor magnetic-geared PM machines are highlighted in [57] and [58].

In [59], Jian et al. presented a magnetic-geared PM machine with a sandwiched armature stator for wind power generation as shown in Figure 10(h). In this machine, the middle component

servers as an armature stator and a flux modulator simultaneously. It was found that this machine exhibits high torque density since PMs on the two rotors are all effectively working in energy conversion process. High power factor is also achieved due to weak armature-excited field.

In [60], Liu et al. presented a double-stator magnetic-geared PM machine for wind power generation, as shown in Figure 10(i). It was shown that high torque density is achieved for this machine due to double-stator arrangement. However, the multi-slot structure increases difficulties in winding coils and manufacturing process. In [61], Zhao and Niu also presented a double-stator magnetic-geared PM machine, as shown in Figure 10(j). In this machine, armature windings are located in the outer stator, while the inner stator is wound by field windings. The pole-pair number of inner excitation sources can be flexibly changed by injecting variable DC field currents. Hence, an effective magnetic field adjustment is achieved by regulating dominant pole-pair flux components. As a result, torque density and flux-regulation capability of this machine are both improved.

3.6 | Comprehensive comparisons

It is always interesting to assess the pros and cons of electric machines for wind power generation. Comprehensive comparisons for conventional electric machines have been summarised in Table 2. It is shown that PMSM machines outperform other conventional electric machines, e.g. SCIMs, WRIMs, and DFIMs, in terms of torque density, efficiency, reliability etc. Hence, the following parts will cover the key publications addressing performance comparisons of various PMSMs, including conventional surface-mounted PMSMs, Vernier PM machines, FSPM machines, FRPM machines, and magnetic-geared PM machines.

In [62], Gerber and Wang compared a Vernier PM machine and a conventional surface-mounted PMSM. It was shown that Vernier PM machine exhibits high output torque capability, which is a good alternative for low-speed high-torque applications, e.g. wind power generation. However, Vernier PM machines suffer from low power factor and high voltage regulation factor [21].

In [63], Zhang et al. conducted a comparative study between several low-speed FSPM machines and surface-mounted PMSMs for direct-drive wind turbines. The results showed that FSPM machines have about 120% torque density with 78% cost per kilowatt as compared to PMSMs. In [64], Shao et al. compared a 12-phase 24/22-p FSPM machine with a 24/22-p surface-mounted PMSM as well as a 48/20-p surface-mounted PMSM for direct-drive wind power generation. It was found that the 24/22-p FSPM machine exhibits the lowest output voltage harmonics and torque ripples, while the 48/20-p surface-mounted PMSM exhibits a lower voltage regulation factor, a higher over-load capability, and a wider operating speed range with high efficiency. In [65], Dobzhanskyi et al. compared a transverse-flux FSPM machine and a surface-mounted PMSM with multi-layer windings. It was found that the surface-mounted PMSM shows higher torque density and efficiency than its counterpart.

In [43], More et al. compared an FRPM machine and a conventional PMSM with fractional-slot concentrated windings. It was shown that although both machines are suitable for low-speed low-power direct-drive application such as rooftop wind generators, the power density of the FRPM machine is approximately 1.5 times that of the investigated PMSM for the same physical dimensions. In [66], Li et al. conducted a comparative study between an FRPM machine and a Vernier PM machine. The results show that the Vernier PM machine is more likely to have higher torque density than the FRPM machine, due to the utilised large DC component of air-gap permeance. In addition, the performance characteristics of the FRPM machine are shown to be more sensitive to the designed parameters, e.g. PM thickness and slot width ratio. In [67], Taras et al. compared an FRPM machine and an FSPM machine, both of which are stator–PM machines. It was shown that the FRPM machine exhibits higher torque density and better fault-tolerant capability in limiting the short-circuit current.

In [57], Kjaer et al. compared an inner-rotor magnetic-geared PM machine and a surface-mounted PMSM. It was shown that with the same output performance, the size, weight, and PM usage of magnetic-geared PM machine are reduced as compared to those of PMSM counterpart. Torque density is significantly improved, i.e. 48.0 versus 8.3 N·m/L for the magnetic-geared PM machine and PMSM, respectively. These performance characteristics indicate there is a promising potential for magnetic-geared PM machines used in direct-drive wind turbines. In [62], Gerber and Wang concluded torque density of magnetic-geared machines is higher than that of Vernier PM machines.

Table 3 summarises a qualitative comparison among various PM machines for wind power generation. These machines include conventional surface-mounted PMSMs, Vernier PM machines, FSPM machines, FRPM machines, and magnetic-geared PM machines. It should be noted that the Vernier PM machines, FSPM machines, FRPM machines, and magnetic-geared PM machines share the same torque production principle, i.e. magnetic-gearing effect and air-gap field modulation [68], [69]. It should also be noted that these new entrants/variants of PMSMs, i.e. Vernier PM machines, FSPM machines, FRPM machines, and magnetic-geared PM machines, are still not commercially available in wind turbine market, although they have been drawing more and more attention in academia. However, reviewing on these machines is of paramount importance for both researchers in academia and engineers in industry since they have shown attractive merits as above mentioned and may provide reference/guidance for manufactures.

4 | SENSORLESS CONTROL METHODS FOR WIND GENERATORS

In variable-speed wind energy conversion systems (WECSs), power electronics units are usually employed for a better control of the input power and grid interaction. For example,

TABLE 3 Comparison of PMSMs in wind power generation

	Surface-mounted PMSM	Vernier PM machine	FSPM machine	FRPM machine	Magnetic-geared PM machine
PM location	Mounted on surface of rotor.	Mounted on surface of rotor.	Sandwiched by stator teeth.	Mounted on surface of stator tooth.	Generally mounted on surface of rotor.
Operating principle	Attraction between magnetic poles from stator and rotor.	Flux modulation [68].	Flux modulation [69].	Flux modulation [69].	Flux modulation [68].
Speed range	Variable speed, low-speed application needs more PM poles.	Variable speed, more suitable for low-speed direct-drive wind turbine [21].	Variable speed, more suitable for high-speed wind turbine with gear box due to robust rotor structure [27].	Variable speed, more suitable for low-speed direct-drive wind turbine [43].	Variable speed, more suitable for low-speed direct-drive wind turbine [57].
Gearbox requirement	Optional	No	Optional	No	No
Torque density	Relatively high due to the high-energy PM [12].	Higher than PMSMs due to the additional reluctance torque component produced by the PMs and the slot harmonic component [21].	Higher than PMSMs due to the flux-focusing effects [63].	Higher than PMSMs [43].	Highest due to the multiple working harmonics modulated by the modulation-ring [57].
Maintenance requirement	Relatively low due to the relatively simple and robust structure [3].	Comparable to PMSMs due to the similar topology with PMSMs.	Lower than PMSMs due to the stator PM arrangement [27].	Lower than PMSMs due to the stator PM arrangement [27].	Relatively high due to complex structure.
Power quality	High due to the more sinusoidal output voltage waveform, low voltage regulation [1].	Relatively low due to low power factor and high voltage regulation [21].	Higher than PMSMs due to inherently sinusoidal EMF and lower THD [27].	Relatively low due to high voltage regulation [42].	Comparable to PMSMs [57].
Efficiency	Highest due to the lowest core losses.	Relatively low due to abundant super-harmonics [21].	Low due to much more abundant super-harmonics [68].	Low due to much more abundant super-harmonics [68].	Relatively low due to abundant super-harmonics [68].
Reliability	Relatively High due to the relatively simple and robust structure [3].	Comparable to PMSMs due to the similar topology with PMSMs.	Higher than PMSMs due to physical and magnetic interphase isolation and robust rotor structure [27].	Higher than PMSMs due to more robust rotor structure [27].	Relatively low due to complex structure.
Cost	Very high due to the high expensive PM usage.	Comparable to PMSMs.	Lower than PMSMs [63].	Lower than PMSMs [43].	Lower than PMSMs due to the low PM usage [57].
Power rating	Both low- and high-power.	Relatively lower than PMSMs, larger power rating machines are rarely investigated.	Both low- and high-power.	Relatively lower than PMSMs, larger power rating machines are rarely investigated.	Relatively lower than PMSMs, larger power rating machines are rarely investigated.

maximum power for a large interval of wind speeds can be extracted, while control of both active and reactive powers into the grid is achieved by means of power electronics [70]. Typical usage of power electronics into WECSs can be categorised into two types, i.e. partial-scale power electronics units [71], [72] and full-scale power electronics units [73]. The control strategies for both the generator-side converter and the grid-side converter have been focused in previous works [2], [74], [75]. In the control system, more advanced features such as the maximum power extraction [76], ride-through operation of the grid faults [77], and providing grid supporting functions in both normal and abnormal operations may be considered. With respect to operation under grid fault, coordinated control of several subsystems in the wind turbine such as the generator/grid side converters, braking chopper/crowbar, and pitch angle controller are necessary [75]. In the available control methods in the generator side, two main control methods, namely tracking of the maximum power without using an anemometer and estimation of rotor position/speed, are emphasised [78]. In recent years, maximum power point tracking (MPPT) methods have been overviewed in many works [79], [80]. Although little work has been reported on position sensorless vector control for AC-generator-based WECSs [81–83], many developed methods in other industrial sensorless AC machine drives can be well transferred into WECS applications [84]. Since permanent magnet synchronous generator (PMSG) is attracting more

attentions in the WECSs and sensorless control methods for different AC machines are similar, sensorless control methods for PMSG-based WECS applications are addressed in this paper.

Most of the sensorless control methods are developed for domestic applications such as electric vehicles and home appliances, where wide operating range is required. Hence, special features are addressed on salient pole, low speed, flux weakening, and good dynamic control. However, in the WECS, the sensorless control methods are more straightforward because of several factors. First, since no power generation below the cut-in wind speed, only the method based on fundamental frequency model is required. Second, the best operating speed is selected according to the MPPT strategy; thus, the speed range is relatively limited. Consequently, generators with small saliency or non-salient pole are preferred. Since the generator speed is usually stable due to mild characteristics of the wind, dynamics of sensorless control method are not highly required.

Among many existing sensorless control methods, the back-EMF observer-based methods and rotor-flux-observer-based methods are most widely applied. After the back-EMFs or rotor flux linkages are observed, extraction methods are needed to detect the position/speed information. This section will review the back-EMF or rotor flux estimation methods as well as the position/speed estimation methods.

4.1 | Back-EMF estimation

The dynamic model of a generic three-phase PMSG can be written in the *dq* reference frame as

$$\begin{cases} u_d = R_s i_d + L_d \left(di_q/dt\right) - \omega_r L_q i_q \\ u_q = R_s i_q + L_q \left(di_q/dt\right) + \omega_r L_d i_d + \omega_r \psi_f \end{cases} \tag{1}$$

where u_{dq}, i_{dq}, and L_{dq} represent armature voltages, armature currents, and inductances in the *dq* reference frame, respectively, R_s is the armature resistance, ψ_f is the flux linkage generated by PMs, and ω_r is the angular velocity of rotor flux.

Although most PMSGs are non-salient-pole, salient-pole PMSGs are also reported in WECSs. To ease the analysis, the concept of extended electromagnetic force (EEMF) is introduced in [85]. Using the inverse Park transformation, dynamics of the PMSG can be modelled in the $\alpha\beta$ stationary reference frame as

$$\mathbf{u}_{\mathrm{fffi}} = R_s \mathbf{i}_{\mathrm{fffi}} + L_d \left(d\mathbf{i}_{\mathrm{fffi}}/dt\right) + \mathbf{e}_{\mathrm{fffi}} \tag{2}$$

where $e_{\alpha\beta}$ represents the EEMF in the $\alpha\beta$ reference frame.

These components can be expressed as

$$\begin{cases} e_\alpha = -e_{ex} \sin\theta_r; e_\beta = e_{ex} \cos\theta_r \\ e_{ex} = \omega_r \psi_f + (L_d - L_q)(\omega_r i_d - \dot{i}_q) \end{cases} \tag{3}$$

where e_{ex} is the magnitude of EEMF.

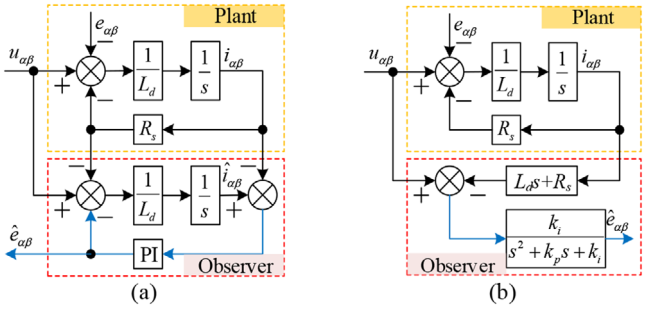

FIGURE 11 Block diagram of the two equivalent linear state observers. (a) Diagram 1. (b) Diagram 2

Since stator voltages and currents are measured, the back-EMF can be obtained by a deadbeat observer, i.e. the algebra calculation of the equations in (2). However, this method is quite sensitive to measurement noise in the stator currents since the derivative of current is used.

To reduce the effect of measurement noise, many state observers are employed to estimate the back-EMF. The existing state observers can be mainly categorised into two types, namely linear state observers and non-linear state observers.

4.1.1 | Linear state observers

The simplest linear state observer is the minimum-order state observer, which is also called as disturbance observer (DOB) in the motion control system. By using the minimum-order state observer, the estimated back-EMF is equivalent to the actual back-EMF, filtered by a first-order low-pass filter (LPF), with its bandwidth is decided by the observer gain.

Since the back-EMF is a sinusoidal signal with a frequency related to the speed, phase delay caused by the first-order LPF varies with the speed. The larger phase delay at higher speed leads to a larger position estimation error though the estimated speed is not affected. To reduce the phase delay, the first-order state observer with a higher bandwidth is required. However, higher bandwidth means poorer noise suppression performance. Therefore, observers with faster dynamics as well as better noise suppression performance are desirable. One alternation is higher order observers. When the sinusoidal back-EMF is taken as one state with assumption of zero derivative, a second-order state observer or linear extended state observer (ESO) is constructed [86], [87]. Using complex vectors, the block diagram of the two equivalent linear state observers is shown in Figure 11.

In the ESO, a proportional–integral (PI) controller is adopted. The estimated back-EMF is the actual back-EMF filtered by a second-order LPF, whose bandwidth is decided by the gains of the PI controller. Since the second-order LPF has a better noise suppression performance than the first-order LPF, the bandwidth of the second-order LPF can be widen to achieve a faster dynamic.

To reduce effect of the disturbance voltage caused by the assumption of zero derivative from back-EMF, a full-order state

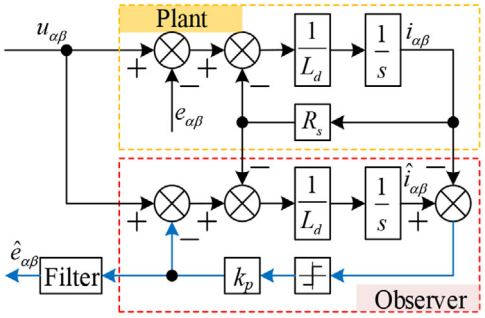

FIGURE 12 Block diagram of the CSMO

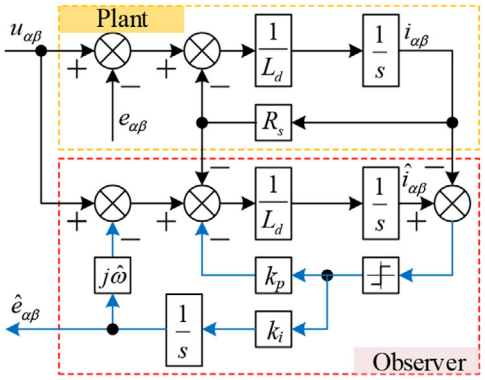

FIGURE 13 Block diagram of the HSMO

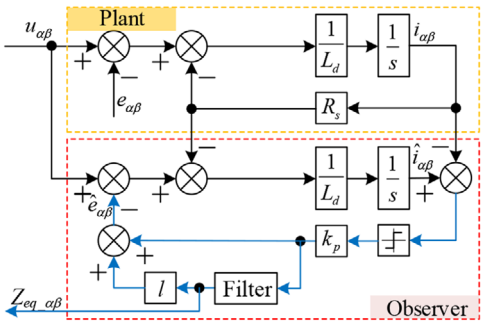

FIGURE 14 Block diagram of the WSMO

observer is proposed in [88]. In the full-order state observer, rotor speed is needed. Since the actual speed is unknown, the estimated speed is used with an adaptive speed estimator.

Though the linear state observers have a nice estimation of disturbance voltages, they are vulnerable to parameter variations [89]. For instance, when the inductance becomes smaller due to magnetic saturation, the estimated back-EMF may also oscillate. Another problem of using the linear state observer comes from the phase delay, which is larger at higher speed. To improve robustness to parameter variations and reduce the phase delay, non-linear observers are preferable.

4.1.2 | Non-linear state observers

In the non-linear observers, sliding-mode observer (SMO) is most widely applied. The SMO has the same robustness to parameter variations as the sliding-mode control, while it consists of different limitation on the controlled objects [90]. Though SMO has a good estimation of the back-EMF without phase delay, it suffers from the chattering problem. The chattering back-EMF cannot be directly used for detection of the position and speed information. In the conventional SMO (CSMO), a first-order LPF is usually employed to derive a less noisy back-EMF. The block diagram of the conventional CSMO is shown in Figure 12.

The adoption of the first-order LPF causes a phase delay. Although the phase delay can be compensated according to the estimated rotor speed, it complicates the algorithm. To overcome the phase delay, Kim et al. [91] used the sigmoid function instead of the signum function with a variable observer gain related to the speed, while Zhao et al. [92] used a saturation function instead of the signum function in discrete-time region. To further improve dynamic estimation performance, Wang et al. [93] proposed a high-order SMO (HSMO), which takes the stator current and the back-EMF as state variables, as shown in Figure 13. Due to the higher order of SMO, the chattering problem caused by usage of the signum function is much alleviated. Consequently, the filter can be avoided. To tackle the speed adaption problem, a quadrature phase-locked loop (PLL) is also proposed.

In the steady state, the back-EMF is proportional to the rotor speed; thus, the observed EEMF in low speed range cannot be used to extract the position and speed information due to the low signal-to-noise ratio (SNR). To expand the speed range, Chi et al. [94] proposed a wide-speed SMO (WSMO), where its block diagram is shown in Figure 14.

If the gain l is set to a negative value, the equivalent control $\tilde{z}_{eq\_\alpha\beta}$ will be larger than the back-EMF. With improved SNR, low-speed operation is possible. The filter used in the observer is a first-order LPF, which is substituted by the adaptive speed estimator as the same as that in [88] to avoid the phase delay [95].

The adaptive speed estimator used in [88] and [95] is also called as the frequency locked-loop (FLL)-based first-order complex vector filter (FOCVF) [96], where its block diagram is shown in Figure 15.

The FLL is widely used in control of grid-connected inverters for detecting the grid frequency. In the FLL, either a PI

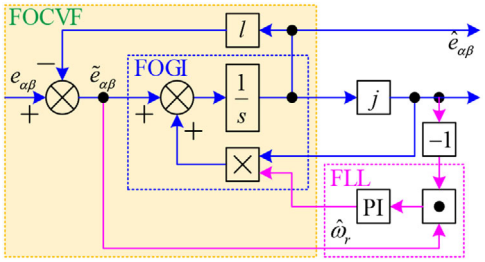

FIGURE 15 Block diagram of FOCVF-FLL

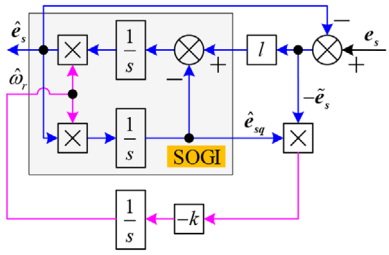

FIGURE 16 Block diagram of SOGI-QSG-FLL

controller is designed based on the Popov's hyperstability theory [88] or a pure integrator is designed based on the Lyapunov's stability theory [95], [97]. The FOCVF is a first-order generalised integrator (FOGI)-based adaptive band-pass filter (BPF), where the centre frequency is the same as the rotor/grid frequency. Consequently, no phase delay is produced at the centre frequency. The observer gain l is used to adjust the quality factor, which affects the bandwidth of the BPF. Consequently, the FOCVF-FLL is appropriate for the detection of signals under unbalanced and distorted operating conditions [98], [99].

Compared with the FOGI-based observer, the second-order generalised integrator (SOGI)-based observer features better filtering characteristics. The SOGI-based observer is first proposed as a quadrature signal generator (QSG) for a single-phase grid-connected inverter [100]. Based on the QSG, the FLL can be realised with single-phase signals [101]. The block diagram of the SOGI-based QSG combined with FLL (SOGI-QSG-FLL) is shown in Figure 16. Due to nice frequency selection characteristics, SOGI-based observers also find applications in the sensorless control system with distorted back-EMF and current [102]. For simplification, these generalized-integrator (GI)-based state observers are called adaptive state observer (ASO).

4.2 | Rotor flux estimation

Similar as the extended back-EMF concept, the active-flux concept turns all salient-pole traveling field machines into non-salient-pole ones. Consequently, a unified state observer for motion-sensorless control can be employed in all AC drives [103]. The d- and q-axis stator flux linkages of the PMSG, i.e. ψ_d and ψ_q, can be expressed by

$$\begin{cases} \psi_d = L_d i_d + \psi_f = L_q i_d + \psi_d^a \\ \psi_q = L_q i_q \end{cases} \tag{4}$$

where $\psi_d^a = \psi_f + (L_d - L_q) i_d$ is the active flux.

Using the inverse Park transformation, stator flux linkages in the $\alpha\beta$ reference frame can be obtained as

$$\begin{bmatrix} \psi_{s\alpha} \\ \psi_{s\beta} \end{bmatrix} = \begin{bmatrix} \cos\theta_r & -\sin\theta_r \\ \sin\theta_r & \cos\theta_r \end{bmatrix} \begin{bmatrix} \psi_d \\ \psi_q \end{bmatrix} = \begin{bmatrix} L_q i_\alpha + \psi_{r\alpha} \\ L_q i_\beta + \psi_{r\beta} \end{bmatrix} \tag{5}$$

where $\psi_{s\alpha\beta}$,$\psi_{r\alpha\beta}$ and $i_{\alpha\beta}$ are the stator flux linkages, rotor flux linkages, and currents in the $\alpha\beta$ stationary reference frame,

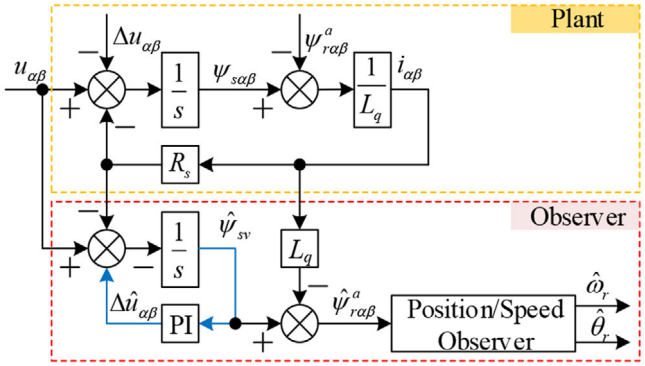

FIGURE 17 Block diagram of rotor flux observers based on low-pass integrator

respectively. The rotor flux linkages can be expressed as

$$\begin{bmatrix} \psi_{r\alpha} \\ \psi_{r\beta} \end{bmatrix} = \psi_d^a \begin{bmatrix} \cos\theta_r \\ \sin\theta_r \end{bmatrix} = \begin{bmatrix} \psi_{s\alpha} - L_q i_\alpha \\ \psi_{s\beta} - L_q i_\beta \end{bmatrix}. \tag{6}$$

The stator flux linkages can be obtained by integration of

$$d\,\psi_{\mathbf{fffi}}/dt = \mathbf{u}_{\mathbf{fffi}} - R_s \mathbf{i}_{\mathbf{fffi}}. \tag{7}$$

The stator flux can be estimated by integration of the voltage equation. Since the voltage model is an essential integrator without any feedback, it is sensitive to offset and drift errors [104]. In practice, an integrator in series with a high-pass filter (also called low-pass integrator) is often used, as shown in Figure 17.

The stator flux-linkage observer is completely insensitive to machine parameters in high-speed range because the resistance voltage drop is less significant relative to the stator voltage though q-axis inductance is used for calculating the rotor flux. Therefore, the linear PI controller, which the gains are easy to tune, is promising [105]. In contradiction to the back-EMF, the rotor flux is independent of the rotor speed. Hence, it can be used in low-speed range [106] and the speed adaption can be avoided. Moreover, the torque and the magnitude of the stator flux can also be estimated at the same time. Consequently, it is easy to integrate the sensorless control with direct torque and flux control [107], [108].

4.3 | Rotor position/speed observers

By selecting a proper method, position/speed-related states such as back-EMF or rotor flux can be obtained. Then, some appropriate detection methods can be employed to detect the position and speed information.

4.3.1 | Direct calculation

If two orthogonal back-EMF components e_α and e_β or rotor flux components $\psi_{r\alpha}$ and $\psi_{r\beta}$ are obtained, the position and

TABLE 4 Comparison of different observers

	Linear state observers		Non-linear state observers			
	DOB	**ESO**	**CSMO**	**WSMO**	**HSMO**	**ASO**
Filter effect	Poor	Good	Medium	Good	Medium	Good
Need phase compensation	Yes	No	Yes	No	No	No
Able to work under unbalancedor distorted condition	No	No	No	No	Yes	Yes
Robustness to parameter variations	Weak	Weak	Strong	Strong	Strong	Strong
Gains setting	Easy	Easy	Easy	Difficult	Difficult	Easy
Algorithm complexity	Simple	Simple	Simple	Complex	Complex	Complex

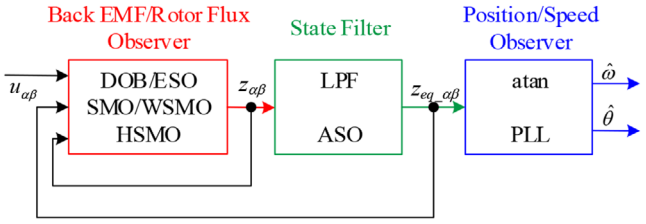

FIGURE 18 Block diagram of general position/speed sensorless control method

speed can be calculated by (8) and (9) as

$$\theta_r = \tan^{-1}\left(-e_\alpha / e_\beta\right) = \tan^{-1}\left(\psi_{r\beta}/\psi_{r\alpha}\right) \tag{8}$$

$$\omega_r = d\theta_r / dt. \tag{9}$$

Although the method is simple and straightforward, it is quite sensitive to the noise in estimated back-EMF or rotor flux. Therefore, better observers for back-EMF or rotor flux are required.

4.3.2 | PLL observer

Commonly, the observer is designed for constant-speed operation; thus, the state equations of position and speed can be expressed as

$$\dot{\theta}_r = \omega_r, \dot{\omega}_r = 0. \tag{10}$$

By selecting different observers, the transfer functions from the position and the speed to their estimations can be changed. The observer acts as a state filter, which is expected to achieve good dynamics as well as nice noise suppression performances. The conventional PLL is designed with an assumption of constant speed, which leads to an estimation error in the case of acceleration or deceleration. Higher gains are beneficial for reducing the estimation error, whereas invokes the problem of bigger noise. There are two types of solutions: one type is non-linear observers [109], [110], while the parameter setting process should be evaluated. The other type is high-order observers [111] with heavier computation burden and perquisition of more knowledge on machine parameters.

According to the structures of all the above-mentioned observers, the block diagram of a general position/speed sensorless control method is shown in Figure 18. A comparison of different observers is shown in Table 4. Linear state observers are easy to implement, while non-linear state observers have stronger robustness to parameter variations. The ASOs have the best filtering characteristics, i.e. no magnitude attenuation and phase delay at the centre frequency, low-frequency disturbance rejection, and thus are promising for machines working under unbalanced and distorted operating conditions.

5 | CHALLENGES

Even though various advanced techniques have been proposed for electric machines and drives in wind power generation systems, design and analysis of these electric machines and drives are still challenging due to existence of non-linearity, strong-coupling, multi-domain physics, and multi-variable. This section will cover the major challenges that electric machines and drives for wind power generation are facing. In particular, modelling difficulties, manufacturing difficulties, electrical failures, and parameter uncertainties are highlighted.

5.1 | Modelling difficulties

Several modelling methods have been developed for design and analysis of electric machines, e.g. analytical models and finite-element analysis (FEA) models. Analytical models are fast, but local saturations and magnetic non-linearity of materials are not taken into account. Hence, low accuracy is the main drawback of analytical models. In the past several decades, numerical FEA models have been widely accepted and utilised in the tasks of electric machine design and analysis, since it can take skin-effects, material non-linearity, as well as mechanical movement of rotor into consideration. However, FEA models are time-consuming due to significant computational burden associated with finite-element (FE) calculations.

For induction machines, including SCIMs, WRIMs, and DFIMs, as aforementioned in Section III, there is a lengthy

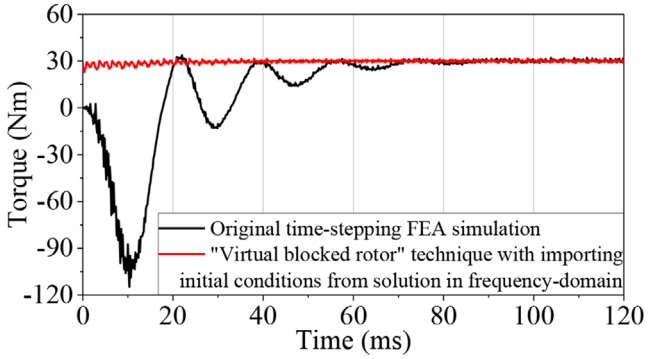

FIGURE 19 Reducing transient response time in FEA simulation of induction machines [114]

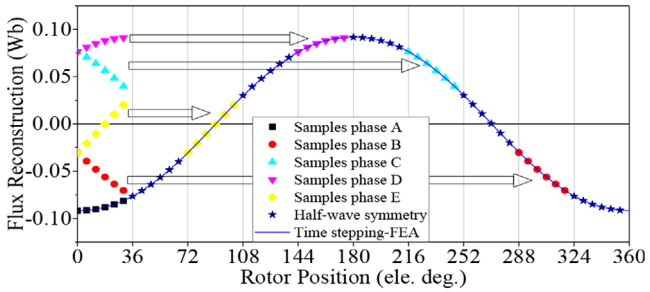

FIGURE 20 Flux-linkage reconstruction procedure by CE-FEA [117]

numerical transient response time during run-up towards a steady state in time-stepping FEA simulation. This lengthy transient response time usually involves use of prodigious amounts of computer resources. Moreover, this indicates a significant impediment to the use of such FEA models in design optimisation of induction machines within reasonable computational time. In order to speed up the FEA transient process, several techniques have been presented. In [112], Lin et al. presented an alternating flux-linkage method with modification of input voltage. In this method, the transient DC flux-linkage component is eliminated by applying an additional voltage component within a small time interval for each phase winding. However, this method may be invalid for induction machines with large leakage inductances. In [113], Räisänen et al. developed a combined method of FEA and time-harmonic analytical models. The solution time of this method is typically small compared to conventional FEA methods, since FE discretisation in the rotor and time integration are avoided. The main limitation of this method is assumption of linear material relations in time-harmonic analytical model, which would inevitably deteriorate simulation accuracy. In [114], Chen et al. presented a so-called virtual blocked rotor technique for simulation of induction machines. In this method, the "virtual blocked rotor" technique in frequency-domain analysis provides an approximation of initial conditions including initial permeabilities and rotor bar currents for FEA transient analysis performed in the time domain. The lengthy simulation transient is significantly reduced with this technique, as shown in Figure 19.

For PM machines, including conventional surface-mounted PMSMs, Vernier PM machines, FSPM machines, and magnetic-geared PM machines, as aforementioned in Section III, no numerical transient in FEA simulation is available yet. However, FEA methods are time-consuming in the early stages of industrial design process, especially in 3D-FEA simulations used for the machines with complex structure. In order to reduce computational burden, efficient automated techniques that can assist researchers/engineers in iterative and tedious simulation process are becoming a necessity. In [115], Gyselinck et al. presented a coupled magnetic equivalent circuit FEA (MEC-FEA) model. Computational effort savings are achieved by this method through employing lumped reluctance elements in locations where the field may exhibit less variation. However, reduction of computational time is limited since the MEC-FEA model will require a full matrix of coefficients that may actually lead to increased computational time. In [116], Ionel et al. presented a so-called computationally efficient FEA (CE-FEA) model for three-phase PMSMs. Afterwards, Chen et al. expanded this model for five-phase FSPM machines in [117] and [118]. The flux-linkage reconstruction procedure is shown in Figure 20. As can be seen, for this five-phase machine, only six magnetostatic FE solutions within a simulated angle of 36 electrical degrees are obtained by FEA simulation. Then, the full flux-linkage waveform is reconstructed by fully exploiting geometric symmetry and time course symmetry of this machine. Hence, up to an order of magnitude of computational time can be saved as compared to conventional time-stepping FEA simulations.

5.2 | Manufacturing difficulties

Manufacturing of electric machines for wind power generation is challenging, especially as they increased in size and complexity. Advanced manufacturing and assembly techniques are imperative in order to achieve the optimal performance of electric machine–drive systems for energy conversion, as well as avoid any potential failures.

Development of induction machines for wind power generation naturally results in larger machine ratings and size. Hence, these types of machines will be installed with larger rotor bar cross sections. However, skin effects in the large rotor bars will be serious, leading to increased rotor resistance that is undesirable. In order to avoid the disadvantages associated with skin effects, reluctance rotors for DFIMs are proposed, which turns out to be doubly fed reluctance machines. A typical doubly fed reluctance machine is shown in Figure 21(a) [119]. Due to absence of rotor windings, doubly fed reluctance machines have the advantage of zero rotor copper losses. Moreover, since the power windings and control windings are naturally decoupled, control of reactive power of these machines is also decoupled. Consequently, complexity of control strategies is greatly reduced [120].

Even though development of rare-earth PM material, e.g. NdFeB, with improved temperature and corrosion resistance in the past several decades has guided the way for

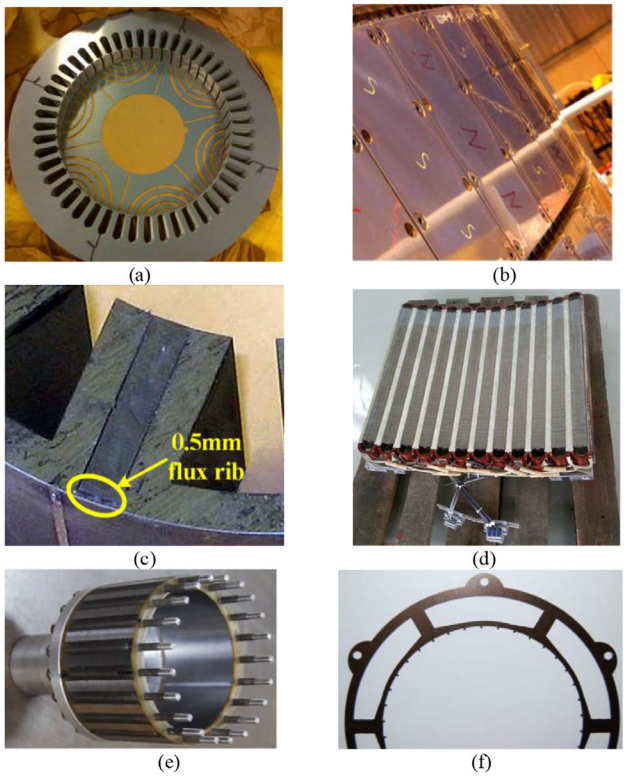

FIGURE 21 Manufacturing parts. (a) Doubly fed reluctance machine laminations for assembly [119]. (b) PM module in a large surface-mounted PMSM [121]. (c) A flux bridge connecting stator segments for a FSPM machine [122]. (d) One stator segment of an FSPM machine [123]. (e) Cup-shaped rotor for a magnetic-geared PM machine [54]. (f) Closed-slot stator for a magnetic-geared PM machine with PM fixed on stator surface [54]

high-performance PM machines, even in large-scaled wind generators, NdFeB PMs are brittle and prone to be pulverised due to intergranular corrosion. In order to prevent intergranular corrosion, PMs with metallurgical microstructure should be appropriately manipulated, e.g. PMs in surface-mounted PMSMs can be protected with hermetically sealed modules, as shown in Figure 21(b) [121].

For FSPM machines, since their complex stator consists of several core segments that are separated by PMs [refer to Figure 8(a)], it is challenging for manufacturing and assembling to make all the stator units to form a perfect circle. In order to ease this manufacturing difficulty, a 0.5-mm-thick flux bridge is added at each of its outer edge of PMs to connect the core segments, as shown in Figure 21(c) [122]. This flux bridge results in an about 1% reduction of output torque due to associated flux leakage. On the other hand, compared to high-speed generators with gearboxes, diameter of direct-drive machines is usually very large, which poses a challenge to manufacturing, transportation, and maintenance. To overcome these aforementioned difficulties, a modular design for an FSPM machine is presented in [123]. In this machine, the stator of the FSPM machine is divided into several segments, as shown in Figure 21(d). Modular stator configuration can ease manufacturing, transportation, as well as installation. Moreover, it is flexible to replace faulty segments with low efforts.

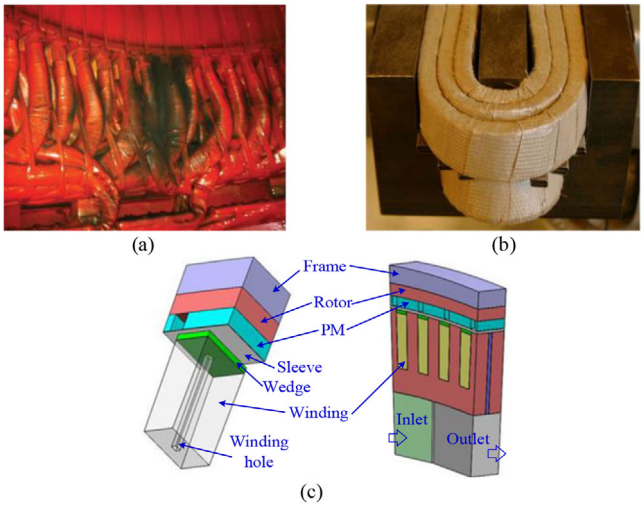

FIGURE 22 Winding issues. (a) A typical winding insulation failure. (b) Stator winding trial showing each turn wrapped in ground-wall insulation [128]. (c) Winding cooling system with radial hole [130]

For magnetic-geared PM machines (refer to Figure 10), stiffness of the modulation ring is a major concern. Manufacturability is mainly affected by mechanical integrity and precision of the rotor. In order to ensure the integrity, the rotor is designed as cup-shaped in [54], as shown in Figure 21(e). In addition, in order to facilitate appropriate mounting of PMs for a magnetic-geared PM machine with PM fixed on the stator surface [refer to Figure 10(d)], a closed-slot stator is designed, as shown in Figure 21(f) [54].

Furthermore, magnetic wedges can be included in stator constructions for all above-mentioned electric machines with open slots, where magnetic wedges in open slot can reduce core losses and improve power factor [124], [125].

5.3 | Electric machine and drive failures

One of the key challenges in wind power generation systems is various electric machine and drive failures. Since repair and maintenance are usually time-consuming and costly, understanding of these failures as well as their associated fault diagnosis methods and fault-tolerant strategies is very important.

The main failures in electric machines and drives for wind power generation are categorised as follows:

1. electrical faults that consist of stator faults including stator winding faults, external drive faults, and rotor faults;
2. thermal faults, e.g. cooling system failure;
3. mechanical faults, e.g. eccentricity faults;
4. magnetic faults, e.g. PM demagnetisation.

Winding insulation failure is the most common fault. It can be caused by overheating, excessive voltage stresses, corrosion etc. A typical winding insulation failure in large-scale wind generators is shown in Figure 22(a). Due to destructive nature and potential propagation, early-stage diagnosis of this fault is

desirable. In [126], Shah et al. presented a diagnostic method of stator inter-turn fault for a DFIM by analysing its rotor current and search-coil voltage. The results show that this method exhibits good capability of timely detection of stator inter-turn fault unambiguously in approximate 2 s, even during speed variations. However, this method is invasive since an extra winding wound on the rotor is required. In [127], based on the Hilbert–Huang transformation, Wang et al. presented an incipient stator insulation fault detection method for PM wind generators. It was shown that this method can detect the very early stage fault in inter-turn insulation by analysing stator current, and the minimum detectable severity degree of inter-turn fault is 0.1488%. On the other hand, in order to prevent and avoid winding fault, ground-wall insulation for a PM generator is used in [128], as shown in Figure 22(b). In this generator, continuous windings are employed in design of a four-series coil per phase to minimise the number of connections and reduce the manufacturing cost.

Since most electric machines for wind power generation are enclosed within a compacted nacelle along with many other devices, both stator and rotor windings need adequate ventilation to keep them functioning properly. Poor ventilation may lead to high winding temperature, which further leads to winding insulation failures and demagnetisation of PMs. In addition to conventional air-forced cooling and liquid cooling technologies, proper cooling design considerations are needed for wind generator design. In [129], Ruuskanen et al. designed radial cooling ducts in both stator and rotor of a PMSM for direct-drive wind power generation. It was found that the stator inductance of this PMSM increases with radial cooling ducts, while the stator stack lamination saturates heavily near cooling ducts due to the increased flux leakage. Based on a thermal resistance network model, optimal number and width of cooling ducts are calculated. In [130], Fan et al. presented coupled fluid-thermal analysis for a 1.5-WM PMSM for wind power generation. The optimal air cooling channels and an alternative cooling structure with radial winding holes through slot centre are designed, so as to dissipate heat from the windings directly, as shown in Figure 22(c). With this artful cooling design, the maximum winding temperature of the investigated PMSM is reduced by about 5 °C.

Eccentricity fault due to bearing bad positioning, weariness, manufacturing imperfections, can result in damages to stator and rotor windings and cores, as well as deteriorate the key performance characteristics, e.g. serious unbalanced magnetic force and cogging torque [128]. Hence, timely diagnosis of eccentricity is essential. In [131], Faiz et al. presented a detection method of eccentricity fault for DFIMs based on the reactive power spectrum. This method is suitable for wind generators since eccentricity fault can be better recognised over low speed. In [132], Bruzzese and Joksimovic presented a diagnostic method of static eccentricities for a salient-pole generator based on harmonic signatures in rotor current. It was shown that a static eccentricity doubles fundamental frequency ripple in the rotor current. This method has advantages of single-sensor measure and accentuated fault sensitivity.

PMs are the key magnetic energy source in various PM machines, which are prone to be irreversibly demagnetised due to high temperature or oversaturation. Hence, PMs have to be protected against magnetic and thermal loads. In [133], Li et al. investigated effects of demagnetisation on electromagnetic field and related parameters in an outer-rotor surface-mounted PMSM for wind power generation. It was found that electromagnetic performance of the PMSM is sensitive to position of the demagnetised PM part. When the demagnetised PM is near to the inner spokes, THD of output voltage becomes large and coefficient of magnetic leakage is increased. In [134], Chen et al. investigated demagnetisation performances of a 7-MW PM wind generator with fractional-slot concentrated windings. It was found that larger slot number per-phase-per-pole and double-layer winding configuration can effectively improve demagnetisation withstand capability.

5.4 | Sensorless control under abnormal conditions

There are two major challenges in designing rotor position/speed sensorless control methods for generators in WECSs. First, problems of harmonics and unbalance will be introduced in the back EMF due to the growth of new types of generators, and the connection between WECS and an unbalanced power grid or load. Therefore, sensorless control methods under unbalanced and distorted back EMF should be studied [135]. Additionally, due to the increasingly complex changing operating conditions, sensorless control methods are required to achieve satisfactory steady-state and dynamic performance over an entire speed range. This requirement, however, cannot be met by a single sensorless control method and may need a combination of different methods [84].

Since GI-based ASOs have good filtering performance and have been proved to be a successful alternation to deal with unbalanced or distorted operating conditions in the grid side [136], [137], they should be able to find more applications in the generator side [138–140]. With the improvement of the microprocessor, it is believed that the combination of non-linear state observers and the ASOs is a good method to deal with different operating conditions. Further studies include the evaluations of the parameter setting principle of non-linear observers as well as the steady-state and dynamic performance of different observers and their combinations.

6 | EMERGING TRENDS AND FUTURE EVOLUTION

In addition to the achievements on the aforementioned advanced electric machines and drives for wind power generation, innovation still continues, which may provide guidance for future evolution of this topic. This section will cover the emerging trends and future evolution of electric machines and drives for wind power generation.

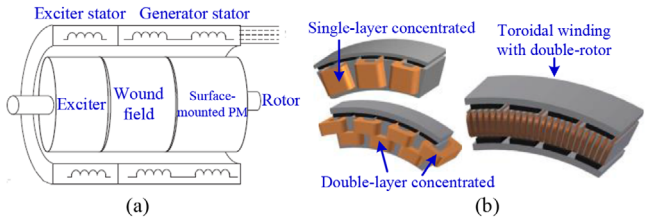

FIGURE 23 Novel PMSMs. (a) Hybrid excited PMSM [141]. (b) Novel winding configurations for surface-mounted PMSM [142]

6.1 | Novel machine topologies

Various novel topologies of electric machines for wind power generation have been developed.

In [141], Beik and Schofield presented a hybrid excited machine, which combines wound field and PM rotor excitations, as shown in Figure 23(a). This is a high-voltage generator with 6.87-kV RMS phase at 600 r/min. The wound field section operates lightly saturated, while the PM section operates unsaturated. This facilitates to improve power density due to a reduced inductance. Moreover, besides conventional overlapping winding configuration in surface-mounted PMSMs, various novel winding configurations are investigated for this kind of machines for wind power generation, including single-layer concentrated windings, double-layer concentrated windings, and toroidal windings with double-rotor structure, as shown in Figure 23(b) [142]. It was shown that with the same output torque performance, the conventional PMSM with overlapping windings has the largest active mass and torque ripple, due to long end windings. The PMSM with single-layer concentrated windings is the easiest model to manufacture and has very high THD of output voltage. Even though the double-rotor PMSM with toroidal windings exhibits the best performance in terms of active mass and PM usage, manufacturing of this machine is the most difficult one. As a result, the PMSM with double-layer concentrated windings is the most favourable topology in the direct-drive wind turbine design.

6.2 | Non-radial-flux machines

Besides conventional radial-flux machines, non-radial-flux machines, i.e. axial-flux machines and transverse-flux machines are gaining interests for wind power generation due to their advantages of short axial length, favourable heat dissipation, and high power density.

In [143], Park et al. presented an axial-flux surface-mounted PMSM for small-scale wind power generation, as shown in Figure 24(a). This machine consists of two rotors and a toroidal winding wound stator. It was shown that the efficiency of this machine is as high as 93.95%. By contrast, in [144], Capponi et al. presented a double-stator single-rotor axial-flux PMSM with fractional-slot concentrated windings, as shown in Figure 24(b). Moreover, different winding configurations are investigated for this machine. It was shown that double-layer

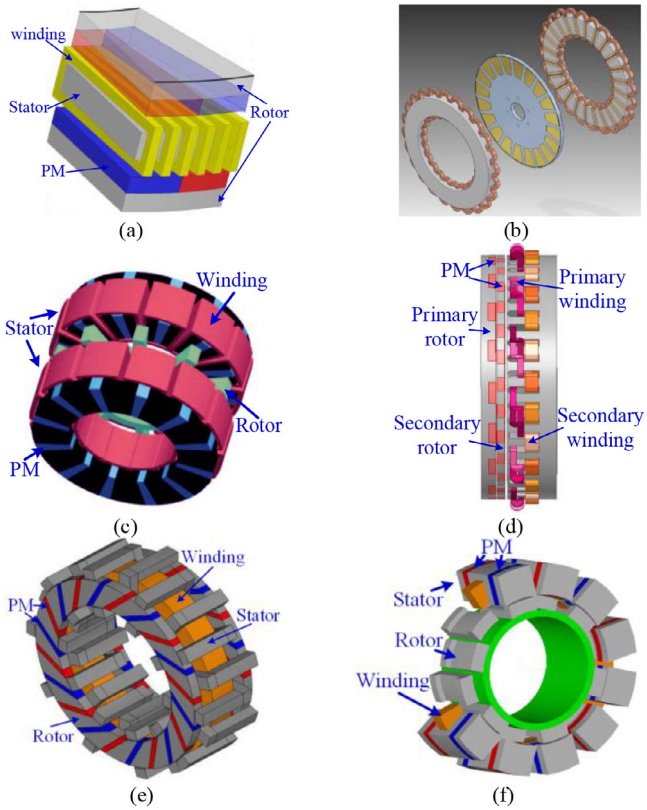

FIGURE 24 Non-radial-flux machines. (a) Axial-flux PMSM [143]. (b) Double-stator single-rotor axial-flux PMSM [144]. (c) Axial-flux FSPM machine [145]. (d) Axial-flux magnetic-geared PM machine [148]. (e) Transverse-flux PM machine [150]. (f) Transverse-flux FSPM machine [151]

winding facilitates to achieve the shortest end connections and low-magnetomotive-force harmonics, compared to the single-layer winding counterpart.

In [145] and [146], Lin et al. presented an axial-flux FSPM machine with a doubly salient structure for direct-drive wind power generation, as shown in Figure 24(c). It was shown that this machine has good prospects in the field of wind power generation, especially in direct-drive wind turbines, due to the unique structure with short axial length and high power density. In [147], Zhao et al. developed an axial-flux dual-rotor FSPM machine for direct-drive wind power generation. It was shown that unaligned arrangement of the two rotors helps to suppress torque ripples within 3.7% and increase flux magnification.

In [148], Niu et al. presented an axial-flux magnetic-geared PM machine for wind power generation, as shown in Figure 24(d). Two sets of windings are adopted in this machine. The primary windings are able to control the secondary rotor at constant rotary speed so that frequency of the secondary winding currents can be maintained constant. This innovative machine shows advantages of compact and integrated structure, enhanced control flexibility, as well as improved efficiency and reliability. In [149], Khatab et al. conducted a comparative study of an axial-flux magnetic-geared PM machine and a conventional axial-flux PMSM. It was shown that the conventional axial-flux PMSM exhibits slightly superior performance

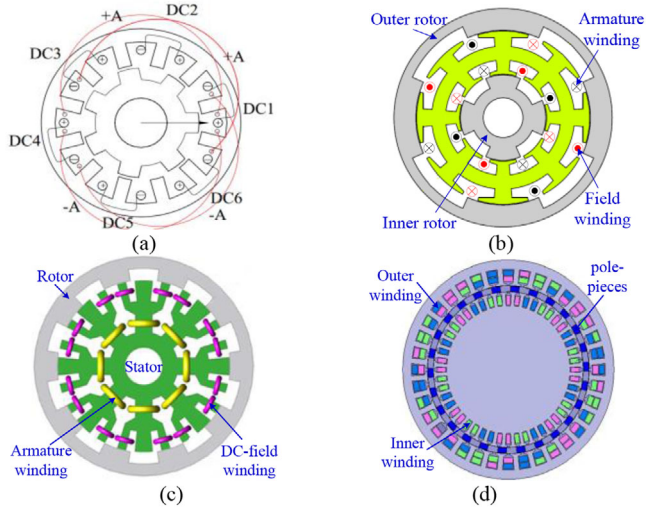

FIGURE 25 Magnetless machines. (a) Magnetless Vernier reluctance machine [156]. (b) Wound-field flux-switching machine [158]. (c) Magnetless flux-reversal machine [160]. (d) Magnetless magnetic-geared machine [161]

under no-load condition, while the axial-flux magnetic-geared PM machine exhibits significantly improvement on torque density (up to 32 kN·m/m^3).

In [150], Jia et al. presented a transverse-flux PM machine for wind power generation, as shown in Figure 24(e). It was shown that this machine processes feature of decoupled electric load and magnetic load, which is favourable to obtain high power density. In [151] and [152], Yan et al. presented a transverse-flux FSPM machine, as shown in Figure 24(f). It indicated that this machine exhibits high torque/power density than its radial- and axial-flux counterparts. Therefore, it is more suitable for direct-drive wind power generation due to reduced weight, cost, and maintenance.

6.3 | Reduced or magnetless machines

Recently, steep increase in the price of high-energy PM materials has triggered researchers/designers to develop machines with less PMs, i.e. reduced or non-rare-earth PM, or fully without PMs [153], [154].

In [155], Jang et al. presented a rare-earth-free surface-mounted PMSM for wind power generation using ferrite PM substituting rare-earth PM, e.g. NdFeB. It was shown that even though ferrite PMSM requires higher PM volumes and a larger number of coil turns with relatively low efficiency, other performance characteristics, e.g. output power, are comparable to conventional NdFeB PMSMs. Moreover, its cost is significantly reduced, which confirms the possibility of substitution of NdFeB PMs with ferrite PMs in wind generators.

In [156], Jia et al. presented a magnetless DC-excited Vernier reluctance machine for wind power generation, as shown in Figure 25(a). It was found that this machine is characterised by low cost due to absence of PMs, high robustness due to simple and robust rotor structure, and wide speed range due to flexible stator DC-exciting field.

In [157], Akuru and Kamper proposed a 12/10-p FSPM machine with ferrite PMs for wind power generation. It was shown that high torque ripples typified by flux-focusing effects of FSPM machines are not enhanced by using rare-earth-free PMs. Moreover, the proposed 3-MW machine offers higher efficiency as compared to conventional rare-earth FSPM counterpart, i.e. 99.11% vs 98.88%. In [158], Yu and Niu developed a single-phase dual-rotor wound-field flux-switching machine for rooftop wind power generation, as shown in Figure 25(b). In this machine, an outer-rotor and an inner-rotor are integrated with a shared stator. It was shown that the developed machine can not only regulate magnetic flux effectively, but also incorporate field and armature windings within one stator to reduce copper losses and improve efficiency. In [159], a 2-MW wound-field flux-switching machine for wind power generation is developed and prototyped. This generator exhibits favourable thermal management since both the field windings and armature windings are located on the stator. It also offers good flux-regulation capability and high torque density. However, this machine would suffer from relatively low efficiency due to additional copper losses from field windings.

In [160], Lee et al. presented a magnetless four-phase flux-reversal machine for wind power generation, as shown in Figure 25(c). It was shown that by utilising the controllable DC-field windings, this machine can control the air-gap flux densities, thus achieving the constant-output-voltage charging characteristics under different conditions. Moreover, with the magnetless structure, this machine enjoys the predominance of cost advantage, compared to its PM counterparts.

In [161], Wang et al. presented a magnetic-geared machine without PMs, as shown in Figure 25(d). In this machine, voltage and frequency of the outer windings are controlled in accordance to speed of the rotor, which is dependent on wind speed. Hence, with the low-speed operation feature of magnetic-geared machines, this machine is particularly suitable for direct-drive wind power generation.

6.4 | Superconducting machines

Superconducting machines are of interest since a very high magnetic field can be produced, which is impossible in conventional machines. High magnetic field results in less machine volume and higher power density. Meanwhile, lack of DC resistance in superconductors contributes to their high efficiency. Moreover, superconducting machines eliminate any need of rare-earth PM materials. Hence, their size and weight are significantly lower as compared to the standard PMSMs. The AMSC and ABB companies have announced to use superconducting machines in their future 10- and 15-MW wind turbines, respectively [162], [163].

In [164], Hsieh et al. presented a 5-MW superconducting EESM for wind power generation, as shown in Figure 26(a). It was found that amount of superconducting material as well as machine volume and weight is significantly affected by air-gap flux density. Hence, key factors, i.e. pole number, rotor radius, and armature reaction, have to be carefully analysed to achieve

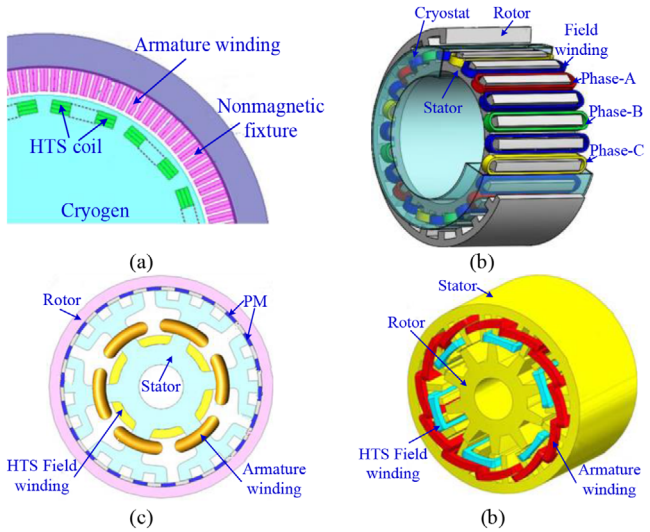

FIGURE 26 Superconducting machines. (a) Superconducting electrically excited machine [164]. (b) Superconducting Vernier reluctance machine [167]. (c) Superconducting Vernier PM machine [168]. (d) Superconducting flux-switching machine [169]

a cost-effective generator. In [165], Snitchler et al. presented a 10-MW superconducting electric machines for wind power generation. It was shown that superconducting technology enables a significant reduction in weight and size as compared to conventional copper and PM-based machines.

In [166], Gao et al. presented a superconducting Vernier machine for wind power generation. Its rotor is installed with high-temperature superconductors as field windings. It was shown that compared to conventional high-temperature superconducting (HTS) machines, this machine can provide higher output torque, lower torque ripple, higher efficiency, and smaller short-circuit current. In [167], Jia et al. presented a superconducting Vernier reluctance machine with concentrated windings for wind power generation. In this machine, both superconducting field and armature windings are located in the stationary stator, as shown in Figure 26(b). It was found that compared to regular superconducting machines, employment of superconducting material is significantly reduced in this machine. In addition, the torque density is 64% higher than conventional direct-drive PM generators, and with lower torque ripple. In [168], Li et al. presented a superconducting Vernier PM machine for wind power generation, as shown in Figure 26(c). In this machine, HTS field windings are wound on the stator yoke. Air-gap flux can be flexibly adjusted by controlling DC from HTS field windings. Hence, output voltage of this machine can be kept as constant under different operating speeds, which is favourable for wind power generation.

In [169], Wang et al. presented a flux-switching machine for wind power generation employing HTS windings for field excitation, as shown in Figure 26(d). It was shown that compared to conventional FSPM counterpart, this machine exhibits higher power density and constant output voltage. Furthermore, they presented a segmented-rotor superconducting flux-switching machine with stationary seal for off-shore wind power generation in [170]. They also presented an axial-flux superconducting flux-switching machine for wind power in [171]. In this machine, a new method is proposed by adjusting rotor relative positions in order to keep its output voltage constant.

It should be noted that expensive material costs and high-standard cooling system are the key challenges in superconducting machines for wind power generation.

7 | CONCLUSION

This paper has presented a comprehensive review of electric machines and drives for wind power generation in terms of challenges and opportunities. Compared to conventional electric machines for wind power generation, including SCIMs, WRIMs, DFIMs, and EESMs, PMSMs are regarded as the most promising candidate. Consequently, advanced PMSMs, i.e. conventional surface-mounted PMSMs, Vernier PM machines, FSPM machines, FRPM machines, and magnetic-geared PM machines, are discussed and compared with emphasis on the key requirements, including torque/power density, efficiency, reliability, cost etc. On the other hand, there are still a lot of technical challenges involved in electric machines and drives to be overcome, while modelling difficulties, manufacturing difficulties, electric machine and drive failures, as well as sensorless control under abnormal conditions are highlighted. However, emerging technologies in electric machines and drives play a major role in making wind power generation systems more efficient, reliable, and cost-efficient.

This paper provides researchers and engineers who are interested in modern electric machines and drives for wind power generation a comprehensive reference and blueprint. It may be helpful to come up with what has been done and may well trigger generation of more innovative ideas in this fast-growing area.

ACKNOWLEDGEMENTS

This work was supported by Start-Up Grant from Nanyang Technological University under Grant 04INS000705C140

REFERENCES

1. Chatterjee, S., Chatterjee, S.: Review on the techno-commercial aspects of wind energy conversion system. IET Renewable Power Gener. 12(14), 1581–1608 (2018)
2. Blaabjerg, F., Liserre, M., Ma, K.: Power electronics converters for wind turbine systems. IEEE Trans. Ind. Appl. 48(2), 708–719 (2012)
3. Yaramasu, V., et al.: High-power wind energy conversion systems: State-of-the-art and emerging technologies. Proc. IEEE 103(5), 740–788 (2015)
4. Nouh, A., et al.: Wind energy conversion systems: classifications and trends in application. In: 5th International Renewable Energy Congress, pp. 1–6 (2014)
5. Bhutto, D.K., et al.: Wind energy conversion systems generators: A review. In: 2nd International Conference on Computing, Mathematics and Engineering Technologies, pp. 1–6 (2019)
6. Li, H., Chen, Z.: Overview of different wind generator systems and their comparisons. IET Renewable Power Gener. 2(2), 123–138 (2008)
7. Muller, S., Deicke, M., De Doncker, R.W.: Doubly fed induction generator systems for wind turbines. IEEE Ind. Appl. Mag. 8(3), 26–33 (2002)
8. Hunt, L.J.: A new type of induction motor. J. Inst. Electr. Eng. 39(186), 648–667 (1907)
9. Strous, T.D., et al.: Brushless doubly-fed induction machines for wind turbines: Developments and research challenges. IET Electr. Power Appl. 11(6), 991–1000, (2017)

10. Han, P., et al.: Brushless doubly-fed machines: Opportunities and challenges. Chin. J. Electr. Eng. 4(2), 1–17 (2018)
11. Ademi, S., et al.: Control of brushless doubly-fed reluctance generators for wind energy conversion systems. IEEE Trans. Energy Convers. 30(2), 596–604 (2015)
12. Gupta, A., et al.: Some investigations on recent advances in wind energy conversion systems. In: 2012 IACSIT Coimbatore Conferences, pp. 47–52 (2012)
13. Sethuraman, L., Dykes, K.L.: GeneratorSE: A sizing tool for variable-speed wind turbine generators. National Renewable Energy Laboratory , Golden, CO, USA, Tech. Rep. TP-5000-66462, 1395455 (2017). https://doi.org/10.2172/1395455
14. Bensalah, A., et al.: Large wind turbine generators: State-of-the-art review. In: XIII International Conference on Electrical Machines, pp. 2205–2211 (2018)
15. Mohammad, S.N., Das, N.K., Roy, S.: A review of the state of the art of generators and power electronics for wind energy conversion systems. In: 3rd International Conference on the Developments in Renewable Energy Technology, pp. 1–6 (2014)
16. He, Y., Chen, X.: Wind turbine generator systems. The supply chain in china: Status and problems. Renewable Energy 34(12), 2892–2897 (2009)
17. Lores, M., Alberto, J.: Evaluación del impacto de los aerogeneradores sobre el radar de vigilancia aérea (2019). [Online]. Available: https://riunet.upv.es/handle/10251/128788
18. Goudarzi, A., Ghayoor, F.: Modelling of wind turbine power curves (WTPCs) based on the sum of the sine functions and improved version of particle swarm optimization (IPSO). In: International SAUPEC/RobMech/PRASA Conference, pp. 1–6 (2020)
19. Keysan, O.: Future electrical generator technologies for offshore wind turbines. Eng. Technol. Ref. 1(1), pp. 1–14 (2015)
20. Bauer, L.: Welcome to wind-turbine-models.com. [Online]. Available: https://en.wind-turbine-models.com
21. Wu, F., El-Refaie, A.M.: Permanent magnet Vernier machine: A review. IET Electr. Power Appl. 13(2), 127–137 (2019)
22. Yu, J., Liu, C., Zhao, H.: Design and multi-mode operation of double-stator toroidal-winding PM Vernier machine for wind-photovoltaic hybrid generation system. IEEE Trans. Magn. 55(7), 1–7 (2019)
23. Zhang, J., et al.: Quantitative design of a high performance permanent magnet Vernier generator. IEEE Trans. Magn. 53(11), 1–4 (2017)
24. Li, J., et al.: A new efficient permanent-magnet Vernier machine for wind power generation. IEEE Trans. Magn. 46(6), 1475–1478 (2010)
25. Kim, B.: Design method of a direct-drive permanent magnet Vernier generator for a wind turbine system. IEEE Trans. Ind. Appl. 55(5), 4665–4675 ((2019)
26. Kim, B.: Design of a direct drive permanent magnet Vernier generator for a wind turbine system. In: IEEE Energy Conversion Congress and Exposition, Portland, OR, USA, pp. 4275–4282 (2018)
27. Chen, H., El-Refaie, A., Demerdash, N.: Flux-switching permanent magnet machines: A review of opportunities and challenges—Part I: Fundamentals and topologies. IEEE Trans. Energy Convers. 35(2), 684–698 (2020)
28. Song, Z., Liu, C.: Induced voltage optimization of a direct-drive multi-phase permanent magnet Vernier generator for tidal energy conversion. In: IEEE PES Asia-Pacific Power and Energy Engineering Conference, pp. 1–5 (2019)
29. Wang, Q., et al.: A new double-winding Vernier permanent magnet wind power generator for hybrid ac/dc microgrid application. IEEE Trans. Magn. 54(11), 8108305 (2018)
30. Hoang, E., Ahmed, H.B., Lucidarme, J.: Switching flux permanent magnet polyphased synchronous machines. In: European Conference on Power Electronics and Applications, pp. 1–8 (1997)
31. Ojeda, J., et al.: Design of a flux-switching electrical generator for wind turbine systems. IEEE Trans. Ind. Appl. 48(6), 1808–1816 (2012)
32. Li, F., et al.: Nine-phase flux-switching permanent magnet brushless machine for low-speed and high-torque applications. IEEE Trans. Magn. 51(3), 8700204 (2015)
33. Shao, L., et al.: A comparative study on nine- and twelve-phase flux-switching permanent-magnet wind power generators. IEEE Trans. Ind. Appl. 55(4), 607–616 (2019)
34. Shao, L., et al.: Mathematical modeling of a 12-phase flux-switching permanent-magnet machine for wind power generation. IEEE Trans. Ind. Electron. 63(1), 504–516 (2016)
35. Shao, L., et al.: Investigation on phase shift between multiple multiphase windings in flux-switching permanent magnet machines. IEEE Trans. Ind. Appl. 53(3), 1958–1970 (2017)
36. Shao, L., et al.: Influence of rotor-pole number on electromagnetic performance in 12-phase redundant switched flux permanent magnet machines for wind power generation. IEEE Trans. Ind. Appl. 53(4), 3305–3316 (2017)
37. Wang, Y., et al.: A controllable power distribution strategy for open winding hybrid excitation generator system. IEEE Trans. Energy Convers. 32(1), 122–136 (2017)
38. Wang, Y., Deng, Z.: Comparison of hybrid excitation topologies for flux-switching machines. IEEE Trans. Magn. 48(9), 2518–2527 (2012)
39. Evans, D.J., et al.: Flux-weakening control performance of partitioned stator-switched flux PM machines. IEEE Trans. Ind. Appl. 52(3), 2350–2359 (2016)
40. Mohamed, E.E.M.: Novel partitioned stator switched flux PM machines for wind generator applications. In: International Conference on Innovative Trends in Computer Engineering, Aswan, Egypt, pp. 427–434 (2018)
41. Deodhar, R.P., Miller, T.J.E.: The flux-reversal machine: A new brushless doubly-salient permanent-magnet machine. IEEE Trans. Ind. Appl. 33(4), 925–934 ((1997)
42. More, D.S., Fernandes, B.G.: Analysis of flux-reversal machine based on fictitious electrical gear. IEEE Trans. Energy Convers. 25(4), 940–947 (2010)
43. More, D.S., Kalluru, H., Fernandes, B.G.: Comparative analysis of flux reversal machine and fractional slot concentrated winding PMSM. In: *34th Annual Conference of IEEE Industrial Electronics*, pp. 1131–1136 (2008)
44. Li, T., et al.: Design of a novel double salient permanent magnet machine for wind power generation. In: International Conference on Electrical Machines and Systems, pp. 1053–1056 (2010)
45. Li, D., et al.: Design and analysis of a flux reversal machine with evenly distributed permanent magnets. IEEE Trans. Ind. Appl. 54(1), 172–183 (2018)
46. More, D.S., Fernandes, B.G.: Power density improvement of three phase flux reversal machine with distributed winding. IET Electr. Power Appl. 4(2), 109–120 (2010)
47. Fernandes, B.G., More, D.S.: Modelling and performance of three-phase 6/14 pole flux reversal machine. IET Electr. Power Appl. 7(2), 131–139 (2013)
48. Dmitrievskii, V.A., et al.: Design and mathematical modeling of gearless smc flux reversal generator for wind turbine. In: International Conference on Electrical Machines, Alexandroupoli, Greece, pp. 2079–2084 (2018)
49. More, D.S., et al.: Outer rotor flux reversal machine for rooftop wind generator. In: IEEE Industry Applications Society Annual Meeting, Edmonton, AB, Canada, pp. 1–6 (2008)
50. Atallah, K., Howe, D.: A novel high-performance magnetic gear. IEEE Trans. Magn. 37(4), 2844–2846 (2001)
51. Crider, J.M., Sudhoff, S.D.: An inner rotor flux-modulated permanent magnet synchronous machine for low-speed high-torque applications. IEEE Trans. Energy Convers. 30(3), 1247–1254 (2015)
52. Jiang, Y., Zhang, J., Li, T.: A permanent magnet brushless doubly fed generator with segmented structure. IEEE Trans. Magn. 54(3), 8700204 (2018)
53. Luo, X., Niu, S.: A novel contra-rotating power split transmission system for wind power generation and its dual MPPT control strategy. IEEE Trans. Power Electron. 32(9), 6924–6935 (2017)
54. Tlali, P.M., Gerber, S., Wang, R.-J.: Optimal design of an outer-stator magnetically geared permanent magnet machine. IEEE Trans. Magn. 52(2), 8100610 (2016)

55. Zhang, X., Liu, X., Chen, Z.: A novel coaxial magnetic gear and its integration with permanent-magnet brushless motor. IEEE Trans. Magn. 52(7), 8203304 (2016)
56. Wang, Q., Niu, S., Yang, S.: Design optimization and comparative study of novel magnetic-geared permanent magnet machines. IEEE Trans. Magn. 53(6), 8104204 (2017)
57. Kjaer, A.B., et al.: Design, fabrication, test, and benchmark of a magnetically geared permanent magnet generator for wind power generation. IEEE Trans. Energy Convers. 35(1), 24–32 (2020)
58. Jian, L., et al.: A magnetic-geared outer-rotor permanent-magnet brushless machine for wind power generation. IEEE Trans. Ind. Appl. 45(3), 954–962 (2009)
59. Jian, L., et al.: Integrated magnetic-geared machine with sandwiched armature stator for low-speed large-torque applications. IEEE Trans. Magn. 48(11), 184–187 (2012)
60. Liu, C., Chau, K.T., Zhang, Z.: Novel design of double-stator single-rotor magnetic-geared machines. IEEE Trans. Magn. 48(11), 4180–4183 (2012)
61. Zhao, X., Niu, S.: Design and optimization of a new magnetic-geared pole-changing hybrid excitation machine. IEEE Trans. Ind. Electron. 64(12), 9943–9952 (2017)
62. Gerber, S., Wang, R.-J.: Design and evaluation of a PM Vernier machine. In: *IEEE Energy Conversion Congress and Exposition*, pp. 5188–5194 (2015)
63. Zhang, J., et al.: Design and comparison of a novel stator interior permanent magnet generator for direct-drive wind turbines. IET Renewable Power Gener. 1(4), 203–210 (2007)
64. Shao, L., et al.: Electromagnetic performance comparison between 12-phase switched flux and surface-mounted PM machines for direct-drive wind power generation. IEEE Trans. Ind. Appl. 56(2), 1408–1422 (2020)
65. Dobzhanskyi, O., et al.: Multilayer-winding versus switched-flux permanent-magnet AC machines for gearless applications in clean-energy systems. IEEE Trans. Ind. Appl. 48(6), 2296–2302 (2012)
66. Li, H.-Y., et al.: Comparative study of air-gap field modulation in flux reversal and Vernier permanent magnet machines. IEEE Trans. Magn. 54(11), 8105206 (2018)
67. Taras, P., et al.: Comparative investigation of stator-mounted permanent magnet machines under fault conditions. J. Eng. 2019(17), 4241–4246 (2018)
68. Zhu, X., et al.: Overview of flux-modulation machines based on flux-modulation principle: Topology, theory, and development prospects. IEEE Trans. Transp. Electrif. 6(2), 612–624 (2020)
69. Zhu, Z.Q.: Overview of novel magnetically geared machines with partitioned stators. IET Electr. Power Appl. 12(5), 595–604 (2018)
70. Blaabjerg, F., et al.: Overview of control and grid synchronization for distributed power generation systems. IEEE Trans. Ind. Electron. 53(5), 1398–1409 (2006)
71. Pena, R., Clare, J.C., Asher, G.M.: Doubly fed induction generator using back-to-back PWM converters and its application to variable-speed wind-energy generation. IEE Proc.—Electr. Power Appl. 143(3), 231–241 (1996)
72. Ekanayake, J.B., et al.: Dynamic modeling of doubly fed induction generator wind turbines. IEEE Trans. Power Syst. 18(2), 803–809 (2003)
73. Chen, Z., Guerrero, J.M., Blaabjerg, F.: A review of the state of the art of power electronics for wind turbines. IEEE Trans. Power Electron. 24(8), 1859–1875 (2009)
74. Anaya-Lara, O., et al.: Wind Energy Generation: Modelling and Control. Wiley, New York, (2009)
75. Blaabjerg, F., Ma, K.: Future on power electronics for wind turbine systems. IEEE J. Emerging Sel. Top. Power Electron. 1(3), 139–152 (2013)
76. Koutroulis, E., et al.: Design of a maximum power tracking system for wind-energy-conversion applications. IEEE Trans. Ind. Electron. 53(2), 486–494 (2006)
77. Morren, J., et al.: Ridethrough of wind turbines with doubly-fed induction generator during a voltage dip. IEEE Trans. Energy Convers. 20(2), 435–441 (2005)
78. Orlando, N.A., et al.: A survey of control issues in pmsg-based small wind-turbine systems. IEEE Trans. Ind. Inf. 9(3), 1211–1221 (2013)
79. Urtasun, A., et al.: Small wind turbine sensorless MPPT: Robustness analysis and lossless approach. IEEE Trans. Ind. Appl. 50(6), 4113–4121 (2014)
80. Yoo, J.I., et al.: Power smoothing of a variable-speed wind turbine generator based on a two-valued control gain. IEEE Trans. Sustain. Energy 11(4), 2765–2774 (2020)
81. Hopfensperger, B., Atkinson, D.J., Lakin, R.A.: Stator-flux-oriented control of a doubly-fed induction machine with and without position encoder. IEE Proc.—Electr. Power Appl. 147(4), 241–250 (2000)
82. Benadja, M., Chandra, A.: Adaptive sensorless control of PMSGs-based offshore wind farm and VSC-HVdc stations. IEEE J. Emerging Sel. Top. Power Electron. 3(4), 918–931 (2015)
83. Abdelrahem, M., et al.: Robust predictive control for direct-driven surface-mounted permanent-magnet synchronous generators without mechanical sensors. IEEE Trans. Energy Convers. 33(1), 179–189 (2018)
84. Zhao, Y., et al.: A review on position/speed sensorless control for permanent-magnet synchronous machine-based wind energy conversion systems. IEEE J. Emerging Sel. Top. Power Electron. 1(4), 203–216 (2013)
85. Morimoto, S., et al.: Sensorless output maximization control for variable-speed wind generation system using IPMSG. IEEE Trans. Ind. Appl. 41(1), 60–67 (2005)
86. Du, B., et al.: Application of linear active disturbance rejection controller for sensorless control of internal permanent-magnet synchronous motor. IEEE Trans. Ind. Electron. 63(5), 3019–3027 (2016)
87. Qu, L., Qiao, W., Qu, L.: An enhanced linear active disturbance rejection rotor position sensorless control for permanent magnet synchronous motors. IEEE Trans. Power Electron. 35(6), 6175–6184 (2020)
88. Chen, Z., et al.: An extended electromotive force model for sensorless control of interior permanent-magnet synchronous motors. IEEE Trans. Ind. Electron. 50(2), 288–295 (2003)
89. Zuo, Y., et al.: Active disturbance rejection controller for speed control of electrical drives using phase-locking loop observer. IEEE Trans. Ind. Electron. 66(3, 1748–1759 (2019)
90. Furuhashi, T., et al.: A position-and-velocity sensorless control for brushless DC motors using an adaptive sliding mode observer. IEEE Trans. Ind. Electron. 39(2, 89–95 (1992)
91. Kim, H., et al.: A high-speed sliding-mode observer for the sensorless speed control of a PMSM. IEEE Trans. Ind. Electron. 58(9), 4069–4077 (2011)
92. Zhao, Y., Qiao, W., Wu, L.: An adaptive quasi-sliding-mode rotor position observer-based sensorless control for interior permanent magnet synchronous machines. IEEE Trans. Power Electron. 28(12), 5618–5629 (2013)
93. Wang, G., et al.: Quadrature PLL-based high-order sliding-mode observer for IPMSM sensorless control with online MTPA control strategy. IEEE Trans. Energy Convers. 28(1), 214–224 (2013)
94. Chi, S., et al.: Sliding-mode sensorless control of direct-drive PM synchronous motors for washing machine applications. IEEE Trans. Ind. Appl. 45(2), 582–590 (2009)
95. Fan, Y., et al.: Sensorless SVPWM-FADTC of a new flux-modulated permanent-magnet wheel motor based on a wide-speed sliding mode observer. IEEE Trans. Ind. Electron. 62(5), 3143–3151 (2015)
96. Luo, Z., et al.: First-order generalized integrator based frequency locked loop and synchronization for three-phase grid-connected converters under adverse grid conditions. J. POWER Electron. 16(5), 1939–1949 (2016)
97. Qiao, Z., et al.: New sliding-mode observer for position sensorless control of permanent-magnet synchronous motor. IEEE Trans. Ind. Electron. 60(2), 10–19 (2013)
98. Yuan, X., et al.: Stationary-frame generalized integrators for current control of active power filters with zero steady-state error for current harmonics of concern under unbalanced and distorted operating conditions. IEEE Trans. Ind. Appl. 38(2, (2002)
99. Rodriguez, P., et al.: Advanced grid synchronization system for power converters under unbalanced and distorted operating conditions. In: *32nd Annual Conference on IEEE Industrial Electronics*, pp. 5173–5178 (2006)

100. Ciobotaru, M., et al.: A new single-phase PLL structure based on second order generalized integrator. In: 37th IEEE Power Electronics Specialists Conference, Jeju, South Korea, pp. 1–6 (2006)
101. Rodríguez, P., et al.: A stationary reference frame grid synchronization system for three-phase grid-connected power converters under adverse grid conditions. IEEE Trans. Power Electron. 27(1), 99–112 (2012)
102. Wang, G., et al.: Enhanced position observer using second-order generalized integrator for sensorless interior permanent magnet synchronous motor drives. IEEE Trans. Energy Convers. 29(2), 486–495 (2014)
103. Boldea, I., Paicu, M.C., Andreescu, G.-D.: Active flux concept for motion-sensorless unified AC drives. IEEE Trans. Power Electron. 23(5), 2612–2618 (2008)
104. Jansen, P.L., Lorenz, R.D.: A physically insightful approach to the design and accuracy assessment of flux observers for field oriented induction machine drives. IEEE Trans. Ind. Appl. 30(1), 101–110 (1994)
105. Foo, G.H.B., Rahman, M.F.: Direct torque control of an ipm-synchronous motor drive at very low speed using a sliding-mode stator flux observer. IEEE Trans. Power Electron. 25(4), 933–942 (2010)
106. Boldea, I., et al.: 'Active flux' DTFC-SVM sensorless control of IPMSM. IEEE Trans. Energy Convers. 24(2), 314–322 (2009)
107. Foo, G., Rahman, M.F.: Sensorless direct torque and flux-controlled IPM synchronous motor drive at very low speed without signal injection. IEEE Trans. Ind. Electron. 57(1), 395–403 (2010)
108. Zhang, Z., et al.: A space-vector-modulated sensorless direct-torque control for direct-drive PMSG wind turbines. IEEE Trans. Ind. Appl. 50(4), 2331–2341 (2014)
109. Yan, J., et al.: Improved sliding mode model reference adaptive system speed observer for fuzzy control of direct-drive permanent magnet synchronous generator wind power generation system. IET Renewable Power Gener. 7(1), 28–35 (2013)
110. Abdelrahem, M., Hackl, C.M., Kennel, R.: Finite position set-phase locked loop for sensorless control of direct-driven permanent-magnet synchronous generators. IEEE Trans. Power Electron. 33(4), 3097–3105 (2018)
111. Lorenz, R.D., Van Patten, K.W.: High-resolution velocity estimation for all-digital, AC servo drives. IEEE Trans. Ind. Appl. 27(4), 701–705 (1991)
112. Lin, D., et al.: Fast methods for reaching AC steady state in FE transient analysis. In: *IEEE International Electric Machines and Drives Conference*, pp. 1–6 (2017)
113. Räisänen, V., et al.: Rapid computation of harmonic eddy-current losses in high-speed solid-rotor induction machines. IEEE Trans. Energy Convers. 28(3), 82–90 (2013)
114. Chen, H., et al.: Fast steady-state analysis in time-stepping finite-element simulation of induction motors based on virtual blocked rotor techniques. IEEE Trans. Ind. Appl. 56(4), 3731–3743 (2020)
115. Gyselinck, J., et al.: Hybrid magnetic equivalent circuit-finite element modeling of transformer fed electrical machines. Int. J. Comput. Math Electr. Electron. Eng. 22(3), 643–658, (2003)
116. Ionel, D.M., et al.: Ultrafast finite-element analysis of brushless PM machines based on space-time transformations. IEEE Trans. Ind. Appl. 47(2), 744–753 (2011)
117. Chen, H., et al.: Comparison and design optimization of a five-phase flux-switching PM Machine for in-wheel traction applications. IEEE Trans. Energy Convers. 34(4), 1805–1817 (2019)
118. Chen, H., et al.: Computationally efficient optimization of a five-phase flux-switching PM machine under different operating conditions. IEEE Trans. Veh. Technol. 68(7), 6495–6508 (2019)
119. Knight, A.M., et al.: Brushless doubly-fed reluctance machine rotor design. In: IEEE Energy Conversion Congress and Exposition, Raleigh, NC, USA, pp. 2308–2315 (2012)
120. Ademi, S., et al.: Theoretical and experimental evaluation of vector control for doubly-fed reluctance generators. In: *International Conference on Electrical Machines*, pp. 936–942 (2014)
121. Kurronen, et al.: Challenges in applying permanent magnet (PM) technology to wind power generators. In: *European Wind Energy Conference & Exhibition*, pp. 4384–4385 (2010)
122. Owen, R.L., et al.: Alternate poles wound flux-switching permanent-magnet brushless AC machines. IEEE Trans. Ind. Appl. 46(2), 790–797 (2010)
123. Ditmanson, C., et al.: A new modular flux-switching permanent-magnet drive for large wind turbines. IEEE Trans. Ind. Appl. 50(6), 3787–3794 (2014)
124. Abdi, S., et al.: Investigation of magnetic wedge effects in large-scale BDFMs. In: *2nd IET Renewable Power Generation Conference*, pp. 1–4 (2013)
125. Shipurkar, U., et al.: A review of failure mechanisms in wind turbine generator systems. In: *17th European Conference on Power Electronics and Applications*, pp. 1–10 (2015)
126. Shah, D., Nandi, S., Neti, P.: Stator-interturn-fault detection of doubly fed induction generators using rotor-current and search-coil-voltage signature analysis. IEEE Trans. Ind. Appl. 45(5), 1831–1842 (2009)
127. Wang, C., Liu, X., Chen, Z.: Incipient stator insulation fault detection of permanent magnet synchronous wind generators based on Hilbert–Huang transformation. IEEE Trans. Magn. 50(11), 8206504 (2014)
128. EL-Refaie, A.M., et al.: High-power-density fault-tolerant PM generator for safety-critical applications. IEEE Trans. Ind. Appl. 50(3), 1717–1728 (2014)
129. Ruuskanen, V., et al.: Effect of radial cooling ducts on the electromagnetic performance of the permanent magnet synchronous generators with double radial forced air cooling for direct-driven wind turbines. IEEE Trans. Magn. 49(6), 2974–2981 (2013)
130. Fan, X., et al.: Ventilation and thermal improvement of radial forced air-cooled FSCW permanent magnet synchronous wind generators. IEEE Trans. Ind. Appl. 53(4), 3447–3456 (2017)
131. Faiz, J., et al.: Detection of mixed eccentricity fault in doubly-fed induction generator based on reactive power spectrum. IET Electr. Power Appl. 11(6), 1076–1084 (2017)
132. Bruzzese, C., Joksimovic, G.: Harmonic signatures of static eccentricities in the stator voltages and in the rotor current of no-load salient-pole synchronous generators. IEEE Trans. Ind. Electron. 58(5), 1606–1624 (2011)
133. Li, W., et al.: Effect of demagnetization fault on electromagnetic field and related parameters in permanent magnet wind generator. In: 22nd International Conference on Electrical Machines and Systems, Harbin, China, pp. 1–7 (2019)
134. Chen, H., et al.: Demagnetization performance of a 7 MW interior permanent magnet wind generator with fractional-slot concentrated windings. IEEE Trans. Magn. 51(11), 8205804 (2015)
135. Zhang, L., et al.: Fault-tolerant sensorless control of a five-phase FTFSCW-IPM motor based on a wide-speed strong-robustness sliding mode observer. IEEE Trans. Energy Convers. 33(1), 87–95 (2018)
136. Golestan, S., et al.: Modeling, tuning, and performance comparison of second-order-generalized-integrator-based FLLs. IEEE Trans. Power Electron. 33(12), 10229–10239 (2018)
137. Zhong, Q.-C., Weiss, G.: Synchronverters: Inverters that mimic synchronous generators. IEEE Trans. Ind. Electron. 58(4), 1259–1267 (2011)
138. Liu, Y., et al.: Sensorless control of standalone brushless doubly fed induction generator feeding unbalanced loads in a ship shaft power generation system. IEEE Trans. Ind. Electron. 66(1), 739–749 (2019)
139. Wu, C., et al.: Adaptive repetitive control of DFIG-DC system considering stator frequency variation. IEEE Trans. Power Electron. 34(4), 3302–3312 (2019)
140. Xu, W., et al.: Improved nonlinear flux observer-based second-order SOIFO for PMSM sensorless control. IEEE Trans. Power Electron. 34(1), 565–579 (2019)
141. Beik, O., Schofield, N.: High-voltage hybrid generator and conversion system for wind turbine applications. IEEE Trans. Ind. Electron. 65(4), 3220–3229 (2018)
142. Potgieter, J.H.J., et al.: Design optimization of directly grid-connected PM machines for wind energy applications. IEEE Trans. Ind. Appl. 51(4), 2949–2958 (2015)
143. Park, Y.-S., et al.: Characteristic analysis on axial flux permanent magnet synchronous generator considering wind turbine characteristics

according to wind speed for small-scale power application. IEEE Trans. Magn. 48(11), 2937–2940 (2012)
144. Giulii Capponi, F., et al.: Fractional-slot concentrated-winding axial-flux permanent-magnet machine with tooth-wound coils. IEEE Trans. Ind. Appl. 50(4), 2446–2457 (2014)
145. Lin, M., et al.: A novel axial field flux-switching permanent magnet wind power generator. IEEE Trans. Magn. 47(10), 4457–4460 (2011)
146. Hao, L., et al.: Static characteristics analysis and experimental study of a novel axial field flux-switching permanent magnet generator. IEEE Trans. Magn. 48(11), 4212–4215 (2012)
147. Zhao, W., Lipo, T.A., Kwon, B.: A novel dual-rotor, axial field, fault-tolerant flux-switching permanent magnet machine with high-torque performance. IEEE Trans. Magn. 51(11), 8112204 (2015)
148. Niu, S., et al.: Development of a novel brushless power split transmission system for wind power generation application. IEEE Trans. Magn. 50(11), 8203004 (2014)
149. Khatab, M.F.H., et al.: Comparative study of novel axial flux magnetically geared and conventional axial flux permanent magnet machines. China Electrotech. Soc. Trans. Electr. Mach. Syst. 2(4), 392–398 (2019)
150. Jia, Z., et al.: A novel transverse flux permanent magnet generator with double c-hoop stator and flux-concentrated rotor. IEEE Trans. Magn. 51(11), 8700704 (2015)
151. Yan, J., et al.: Magnetic field analysis of a novel flux switching transverse flux permanent magnet wind generator with 3-D FEM. In: *International Conference on Power Electronics and Drive Systems*, pp. 332–335 (2009)
152. Yan, J., et al.: Cogging torque optimization of flux-switching transverse flux permanent magnet machine. IEEE Trans. Magn. 49(5), 2169–2172 (2013)
153. Boldea, I., Tutelea, L., Blaabjerg, F.: High power wind generator designs with less or no PMs: An overview. In: *17th International Conference on Electrical Machines and Systems*, pp. 1–14 (2014)
154. Chau, K.T., Liu, C., Lee, C.H.T.: Design and analysis of a dual-mode flux-switching doubly salient DC-field magnetless machine for wind power harvesting. IET Renewable Power Gener. 9(8), 908–915 (2015)
155. Jang, S.-M., et al.: Design and electromagnetic field characteristic analysis of 1.5 kw small scale wind power generator for substitution of Nd-Fe-B to ferrite permanent magnet. IEEE Trans. Magn. 48(11), 2933–2936 (2012)
156. Jia, S., Qu, R., Li, J.: Analysis of the power factor of stator dc-excited Vernier reluctance machines. IEEE Trans. Magn. 51(11), 8207704 (2015)
157. Akuru, U.B., Kamper, M.J.: Intriguing behavioral characteristics of rare-earth-free flux switching wind generators at small- and large-scale power levels. IEEE Trans. Ind. Appl. 54(6), 5772–5782 (2018)
158. Yu, C., Niu, S.: Development of a magnetless flux switching machine for rooftop wind power generation. IEEE Trans. Energy Convers. 30(4), 1703–1711 (2015)
159. Cao, R. et al.: MW-class stator wound field flux-switching motor for semidirect drive wind power generation system. IEEE Trans. Ind. Electron. 66(1), 795–805 (2019)
160. Lee, C.H.T., Chau, K.T., Liu, C.: Design and analysis of a cost-effective magnetless multiphase flux-reversal DC-field machine for wind power generation. IEEE Trans. Energy Convers. 30(4), 1565–1573 (2015)
161. Wang, Y., et al.: A novel brushless doubly fed generator for wind power generation. IEEE Trans. Magn. 48(11), 4172–4175 (2012)
162. Terao, Y., Sekino, M., Ohsaki, H.: Comparison of conventional and superconducting generator concepts for offshore wind turbines. IEEE Trans. Appl. Supercond. 23(3), 5200904 (2013)
163. Qu, R., Liu, Y., Wang, J.: Review of superconducting generator topologies for direct-drive wind turbines. IEEE Trans. Appl. Supercond. 23(3), 5201108 (2013)
164. Hsieh, M.-F., et al.: Design and analysis of high temperature superconducting generator for offshore wind turbines. IEEE Trans. Magn. 49(5), 1881–1884 (2013)
165. Snitchler, G., et al.: 10 MW class superconductor wind turbine generators. IEEE Trans. Appl. Supercond. 21(3), 1089–1092 (2011)
166. Gao, Y., et al.: HTS Vernier machine for direct-drive wind power generation. IEEE Trans. Appl. Supercond. 24(5), 5202905 (2014)
167. Jia, S., et al.: A novel Vernier reluctance fully superconducting direct drive synchronous generator with concentrated windings for wind power application. IEEE Trans. Appl. Supercond. 26(7), 5207205 (2016)
168. Li, W., Ching, T.W., Chau, K.T.: A new high-temperature superconducting Vernier permanent-magnet machine for wind turbines. IEEE Trans. Appl. Supercond. 27(4), 5202905 (2017)
169. Wang, Y., et al.: Design and analysis of a HTS flux-switching machine for wind energy conversion. IEEE Trans. Appl. Supercond. 23(3), 5000904 (2013)
170. Wang, Y., et al.: Design, analysis, and experimental test of a segmented-rotor high-temperature superconducting flux-switching generator with stationary seal. IEEE Trans. Ind. Electron. 65(11), 9047–9055 (2018)
171. Wang, Y., et al.: Design and analysis of a new HTS axial-field flux-switching machine. IEEE Trans. Appl. Supercond. 25(3), 5200905 (2015)

How to cite this article: Chen H, Zuo Y, Chau KT, Zhao W, Lee CHT. Modern electric machines and drives for wind power generation: A review of opportunities and challenges. *IET Renew. Power Gener.* 2021;15:1864–1887.
https://doi.org/10.1049/rpg2.12114